On growth and form of the mammary gland: Mesenchyme instructs growth while epithelium directs branching

Qiang Lan[1], Ewelina Trela[1], Riitta Lindström[1], Jyoti Satta[1], Beata Kaczyńska[1], Mona M. Christensen[1], Martin Holzenberger[2], Jukka Jernvall[1,3], Marja L. Mikkola[1]

[1] Cell and tissue dynamics research program, Institute of Biotechnology, Helsinki Institute of Life Science (HiLIFE), University of Helsinki, Finland

[2] Sorbonne University, INSERM, Research Center Saint-Antoine, Paris, France

[3] Department of Geosciences and Geography, University of Helsinki, Helsinki, Finland

Corresponding Author: Marja L. Mikkola, marja.mikkola@helsinki.fi

Conflict of interest statement: The authors have no conflicts of interest to declare.

Keywords: mammary gland, salivary gland, mesenchyme, embryonic development, Eda, Wnt, IGF-1, IGF-1R, branching morphogenesis

Abstract

Mammary gland is a unique organ that undergoes dynamic alterations throughout a female's reproductive life, making it an ideal model for developmental, stem cell and cancer biology research. Mammary gland development begins *in utero* and proceeds via a quiescent bud stage before the initial outgrowth and subsequent branching morphogenesis. How mammary epithelial cells transit from quiescence to an actively proliferating and branching tissue during embryogenesis and, importantly, how the branch pattern is determined remain largely unknown. Here we provide evidence indicating that epithelial cell proliferation, segregation into basal and luminal lineages that characterize the postnatal mammary duct, and onset of branching are independent processes, yet partially coordinated by the Eda signaling pathway. By performing heterotypic and heterochronic epithelial-mesenchymal recombination experiments between mammary and salivary gland tissues and *ex vivo* live imaging, we demonstrate that unlike previously concluded, the mode of branching is an intrinsic property of the mammary epithelium while the growth pace and density of the mammary ductal tree are governed by the mesenchyme. Transcriptomic profiling and *ex vivo* and *in vivo* functional studies disclose that mesenchymal Wnt/ß-catenin signaling, and in particular IGF-1 downstream of it critically regulate mammary gland growth. These results underscore the general need to carefully decompose the different developmental processes producing branched organs.

Introduction

Branching morphogenesis is a common developmental process driving the formation of a number of organs including lung, kidney, salivary and mammary gland [1]. Although some fundamental principles are shared, each organ employs its unique branching strategy – mode and density of branching – to achieve the proper architecture tailored to its function [1-3]. In recent decades, significant advancements have been made in unraveling the underlying mechanisms of branching morphogenesis in various organs and species. However, many questions remain unanswered, especially regarding the mammary gland as much of the research focus has been on its postnatal growth[1, 2]. Yet, mammary gland morphogenesis commences already during fetal life by formation of placodes, local epithelial thickenings, in the flanks of the fetus. How these early steps of branching morphogenesis differ between mammary gland and other organs remains poorly understood.

In mice, five pairs of mammary placodes emerge around embryonic day 11 (E11). Placodes invaginate by E13 giving rise to buds that are now surrounded by condensed, mammary-specific mesenchyme [4-6]. Mammary buds stay relatively non-proliferative until E15-E16 when they sprout toward the adjacent 'secondary' mammary mesenchyme, the fat pad precursor tissue that later gives rise to the adult stroma. Branching begins at E16, and by E18 (1-2 days prior to birth) mammary rudiments have developed into small ductal trees with 10-25 branches [3, 7]. In contrast to the postnatal bilayered mammary epithelium consisting of outer basal and inner luminal cells, embryonic mammary rudiments undergo branching as a solid mass of epithelial cells without lumen. Mammary rudiments initially consist of multipotent precursors that become restricted to basal and luminal lineages during later stages of embryogenesis [8, 9]. The mechanisms governing the exit from quiescence and acquisition of branching ability are still enigmatic. The observation that the

64 initial outgrowth coincides with activation of proliferation and lineage segregation has led to
65 the hypothesis that they might be functionally connected [8, 10]. However, whether a causal
66 link exists between these phenomena is currently unknown.

67 Reciprocal epithelial-mesenchymal tissue interactions are critical for mammary
68 gland development at all stages. Many signaling pathways essential for mammary placode
69 and bud formation have been identified, but the paracrine factors regulating branching
70 during embryogenesis are less well understood [4, 5, 11, 12]. The tumor necrosis factor family
71 member ectodysplasin A1 (Eda) is one such mesenchymal factor: Eda deficiency
72 compromises ductal growth and branching, while mice overexpressing Eda exhibit a
73 dramatic ductal phenotype with precocious sprouting and excessive growth and branching
74 [13, 14]. In addition, the Wnt and fibroblast growth factor (Fgf) pathways are likely involved [7,
75 11], but the early developmental arrest observed in mice where these pathways are
76 inactivated [15, 16] has hampered elucidation of their exact roles during branching
77 morphogenesis.

78 Importantly, the current paradigm posits that the mesenchyme specifies the
79 epithelial branching pattern in all branched organs [1, 3]. This conclusion stems from tissue
80 recombination experiments where epithelia and mesenchymes of different origins have
81 been exchanged: lung mesenchyme instructs the kidney epithelium to adopt a lung-type
82 branching pattern while organ-specific mode of branching is maintained in homotypic
83 tissue recombinants [17, 18]. The same conclusion was drawn from the pioneering
84 experiments involving salivary gland mesenchyme and mammary gland epithelium. Even
85 though the mammary epithelium retained its cellular identity, the branch pattern was
86 reported to be salivary gland-like: branches formed at higher density and by tip clefting
87 rather than lateral branching [19, 20]. In addition, salivary gland mesenchyme promoted much

88 faster growth. Although the evidence from the early experiments appear compelling, the
89 underlying molecular basis remained elusive.
90 To uncover the regulation of mammary gland branching, we first revisited the
91 heterochronic tissue recombination using mammary tissues. Our results show that the
92 timing of the initial branching is epithelium-dependent, yet epithelial-mesenchymal
93 interactions are indispensable for the outgrowth to occur. Further analysis suggests that
94 onset of branching is independent of onset of proliferation and lineage segregation, yet
95 they are partially coordinated by the Eda pathway. In strong contrast to the previous
96 reports and to the paradigm of the role of the mesenchyme in directing branching [19, 20], live
97 imaging disclosed that salivary gland mesenchyme failed to switch the mode of mammary
98 branching into salivary-like. This implies that branch pattern formation is an intrinsic
99 property of the mammary epithelium. Nevertheless, salivary mesenchyme had a major
100 growth-promoting effect on the mammary epithelium once it had acquired branching
101 capacity. Transcriptomic profiling of mammary and salivary gland mesenchymes identified
102 mesenchymal Wnt/ß-catenin pathway and its downstream target *Igf1* as potential drivers
103 of epithelial growth, thereby decomposing mode of branching from growth control in
104 mammary development.
105
106 **Results**
107 **The timing of onset of branching is an intrinsic property of the mammary epithelium**
108 To assess whether timing of the mammary initial branching can be influenced by
109 tissues of different developmental stages, we performed heterochronic epithelial-
110 mesenchymal recombination experiments. To this end, we used tissues micro-dissected
111 from fluorescently labeled transgenic mice allowing day-to-day imaging, as well as
112 evaluation of the purity of the tissue compartments (Fig. 1a). Because anterior mammary

113 glands are more advanced in their development than the posterior ones [7], only mammary
114 glands 1 to 3 were used throughout the study, unless otherwise specified, to avoid any
115 biases caused by the asynchrony.

116 It has been previously shown that early (E12) mammary mesenchyme does not
117 alter the onset of branching of the mammary epithelium (E12 to E16) in *ex vivo* tissue
118 recombination experiments [19]. However, the ability of late mammary mesenchyme to
119 advance epithelial outgrowth and branching has not been assessed. To answer this
120 question, we recombined E13.5 mammary epithelia (quiescent bud stage) with E13.5,
121 E15.5, or E16.5 (when the very first branches are evident) mammary mesenchymes. In the
122 control explants (E13.5 epithelia with E13.5 mesenchyme), branching started after 3-4
123 days of culture (Fig. 1b,c), in good agreement with development *in vivo*. No precocious
124 branching was observed when 'older' mesenchyme was used: when E13.5 epithelia were
125 cultured with either E15.5 or E16.5 mesenchyme, branching was again evident only after
126 3-4 days of culture (Fig. 1b, c). As an additional control, we performed similar experiments
127 as described by Kratochwil [19], and cultured E13.5, E15.5 or E16.5 mammary epithelia with
128 E13.5 mammary mesenchyme (Fig. 1d). As previously reported, all epithelia branched in
129 E13.5 mesenchyme, and outgrowth started after 3-4, 1-2, and 0-1 days of culture,
130 respectively (Fig. 2e), correlating with the stage of epithelium and its developmental pace
131 *in vivo.*

132 Next, we asked whether the mesenchyme is needed for initiation of branching. To
133 this end, we utilized a mesenchyme-free 3D mammary organoid technique to culture
134 micro-dissected intact mammary rudiments in a serum-free medium with growth
135 supplements [21](Fig. 1f). In the 3D Matrigel matrix, E16.5 mammary epithelia generated
136 large branching trees in just 3 days (Fig. 2g,f and Supplementary Fig.1), whereas epithelia
137 from earlier stages (E13.5 to E15.5) consistently failed to branch even after eight days of

138 culture. Some specimens enlarged in size, yet they failed to progress, except for
139 occasional E15.5 epithelia that generated a few branches (Fig. 2g,i and Supplementary
140 Fig. 1).

141 Besides confirming previous observations [19] our results reveal that mesenchymes
142 from advanced developmental stages could not alter the pace of epithelial outgrowth, yet
143 epithelial-mesenchymal interactions are indispensable for the mammary epithelium to
144 acquire branching ability.

145 **Basal-cell biased proliferation is activated in mammary epithelium prior to initiation**
146 **of branching**

147 Next, we sought to determine which mammary epithelial properties are required
148 for the onset of branching. Majority of mammary epithelial cells are quiescent at the
149 placode and bud stages [22-24], and proliferation is thought to resume when branching
150 begins at around E16 [22]. Such coincidence suggests that activation of proliferation may
151 closely cooperate with, or even drive the onset of branching. To gain more insight into the
152 quiescent stage of the embryonic mammary primordium, we first quantified the volume of
153 the mammary epithelium with the aid of 3D surface renderings of EpCAM-stained
154 specimens (Fig. 2a). The volume of mammary rudiments steadily increased from E13.5 to
155 E16.5 (Fig. 2b), whereas quantification of the branch (tip) number showed that active
156 branching did not take place until E16.5 (Fig. 2c).

157 To analyze epithelial proliferation between E13.5 and E16.5, we investigated cell
158 cycle dynamics using the Fucci2a mouse model, where cells in S/G2/M phase of the cell
159 cycle express nuclear mVenus while cells in G1/G0 express nuclear mCherry [25]. The ratios
160 of mammary epithelial cells in S/G2/M and G1/G0 phases were quantified in 3D after
161 whole-mount staining with EpCAM (Fig. 2d). In line with the previous report [24], only ~20%
162 of mammary epithelial cells were in S/G2/M phase at E13.5, with no apparent change at

163 E14.5 (Fig. 2e). However, the proportion of S/G2/M cells significantly increased at E15.5
164 but plateaued and even slightly decreased at E16.5 when branching was evident (Fig. 2e).
165 Initiation of branching morphogenesis has also been proposed to be associated with
166 the onset of basal and luminal lineage segregation at E15-E16 [8]. A recent single-cell RNA
167 sequencing (RNAseq) profiling study identified a cluster of proliferative cells in addition to
168 the luminal and basal cell clusters in the E15.5 mammary gland [26]. These findings
169 prompted us to examine whether the proliferative cells display any bias in their distribution
170 at E13.5-E16.5. Due to the absence of clear spatial segregation of basal and luminal
171 lineage markers during these early developmental stages [9], we instead measured the
172 distance of each nucleus to the surface of epithelial mammary rudiments in 3D to define
173 their location (Fig. 2f). Distribution of all nuclei revealed a cluster of cells localizing within
174 10 μm distance from the epithelial surface (dashed line in Fig. 2g), corresponding well with
175 the confocal images showing radially organized, basally-located elongated cells in the
176 same position (Fig. 2d,f). Next, we stratified the epithelial cells to basal (nuclear distance
177 less than or equal to 10 μm from the surface) and inner ("luminal") (nuclear distance more
178 than 10 μm) ones and quantified the ratios of S/G2/M and G1/G0 cells in each
179 compartment (Fig. 2h). At E13.5 and E14.5, the proportion of S/G2/M cells was higher in
180 the inner compartment, though the difference was statistically significant only at E14.5.
181 However, concomitant with the overall increase in proliferation (Fig. 2e), there was a
182 switch in the proportion of S/G2/M and G1/G0 cells at E15.5 and E16.5, basal cells being
183 significantly more proliferative.

184 **Basal-cell biased proliferation is not sufficient to drive initiation of branching**

185 The observation that basal cell-biased proliferation occurred prior to onset of
186 branching suggests that it might be a prerequisite for branching to occur. Interestingly,
187 activation of epithelial cell proliferation also seems to be associated with basal cell lineage

188 specification. To further investigate the potential link between lineage segregation,
189 proliferation, and initiation of branching, we took advantage of a mouse model that
190 displays precocious onset of branching, the K14-*Eda* mouse overexpressing Eda under
191 the keratin 14 (K14) promoter. Eda and its epithelially-expressed receptor Edar regulate
192 growth and branching of the embryonic and pubertal mammary gland [13, 14, 27, 28]. In K14-
193 *Eda* embryos, mammary epithelial proliferation is increased, and branching is initiated
194 already at E14.5 [13].

195 To more closely examine the cellular alterations induced by Eda, we quantified the
196 size, branch tip number, and proliferation status in K14-*Eda* embryos and their wild type
197 littermates at E13.5 and E14.5. Mammary buds of K14-*Eda* embryos were significantly
198 larger already at E13.5 (Fig. 3a,b), and at E14.5, the volume was comparable to those of
199 E16.5 wild type embryos (compare Fig. 3b to Fig. 2b, all mice in C57Bl/6 background). As
200 reported [13], branching was evident in K14-*Eda* embryos already at E14.5 (Fig. 3c).

201 To specifically assess the link between lineage segregation and onset of branching,
202 we analyzed expression of the well-established basal and luminal markers, keratin 14
203 (K14) and keratin 8 (K8) respectively, in K14-*Eda* and littermate control mammary glands
204 (Supplementary Fig. 2a) between E13.5 and postnatal day 5 (P5). At E13.5, there was no
205 obvious difference between the genotypes. Intriguingly, at E14.5 and E15.5, K14-*Eda*
206 mammary rudiments displayed a notable downregulation of K8 not only in basal cells, but
207 also in inner cells (Supplementary Fig. 2a). However, K8 expression resumed at E16.5,
208 and at P1, and P5, no difference between the genotypes was observed (Supplementary
209 Fig. 2a). Accordingly, gene set enrichment analysis of a microarray dataset of E13.5 *Eda*$^{-/-}$
210 mammary buds treated with recombinant Eda protein for 4 hours [29] revealed a positive
211 enrichment of 'LIM_Mammary_Stem_Cell_Up' gene signature [30], known to represent the
212 basal cell signature (Supplementary Fig. 2b). These data suggest that lineage segregation

213 is unlikely to be a prerequisite for branching to commence, as branching was observed
214 even though luminal lineage was transiently suppressed in K14-*Eda* embryos. However,
215 we cannot exclude the possibility that consolidation of basal fate in basally located cells
216 (by downregulation of luminal fate) plays a role.

217 Next, we focused on investigating the link between proliferation and onset of
218 branching. Analysis of Fucci2a reporter expression in K14-*Eda* embryos at E13.5 and
219 E14.5 revealed that the portion of S/G2/M cells was significantly higher in K14-*Eda* mice at
220 both stages compared with wild type littermates (Fig. 3d and Supplementary Fig. 3a). In
221 addition, the basal cell-biased proliferation was evident already at E14.5 (but not yet at
222 E13.5) in K14-*Eda* embryos (Fig. 3e), similar to wild type mice at E15.5/E16.5 (Fig. 2h).
223 Since E14.5 K14-*Eda* mammary glands had similar characteristics to E16.5 wild type in
224 terms of volume, elevated overall proliferation, and basal cell-biased proliferation, we next
225 tested their ability to grow and branch in the mesenchyme-free 3D Matrigel culture. E14.5,
226 but not E13.5, K14-*Eda* epithelia were able to branch, whereas epithelia isolated from wild
227 type littermates expectedly failed to generate outgrowths (Fig. 3f, g). We also analyzed
228 Fucci2a reporter expression in *Eda*$^{-/-}$ mice [31] at E15.5 and E16.5. As we previously
229 reported [13], loss of *Eda* led to smaller glands and the onset of branching was delayed with
230 most mammary glands being unbranched at E16.5 (Fig. 3h-j). However, the overall
231 proliferation (Fig. 3k), as well as the relative portion of S/G2/M cells in basal and inner cells
232 (Fig. 3l and Supplementary Fig. 3b) were similar between *Eda*$^{-/-}$ and wild type controls at
233 both stages. To evaluate the branching ability, we again performed mesenchyme-free 3D
234 culture. While nearly all E16.5 control epithelia gave rise to branched outgrowths, as
235 expected, about half of *Eda*$^{-/-}$ epithelia failed to do so (Fig. 3m,n).

236 Collectively, these data indicate that initiation of branching succeeds activation of
237 proliferation but is not its direct consequence. Additionally, analysis of K14-*Eda* mammary

238 rudiments suggests that exit from quiescence and branching ability can occur
239 independently of lineage specification.
240
241 **Salivary gland mesenchyme is rich in growth-promoting cues, but does not alter the**
242 **mode of branch point formation of the mammary epithelium**
243 Next, we shifted our focus on the regulation of the branching pattern, which is
244 thought to be determined by mesenchymal cues [19, 20]. To assess the influence of the
245 mesenchyme, we performed heterotypic and heterochronic epithelial-mesenchymal
246 recombination experiments between fluorescently labeled mammary and salivary gland
247 tissues. Mammary epithelia and mesenchymes were isolated either at the quiescent bud
248 stage (E13.5), or right after the bud had sprouted (E16.5); in addition to the primary
249 mesenchyme, also mammary fat pad precursor tissue was micro-dissected from E16.5
250 embryos. Salivary gland tissues were isolated at E13.5, when the first branching events
251 are evident and tissue separation is effortless. Homotypic recombinations were used as
252 controls.
253 As previously reported [19], E16.5 mammary ductal trees were far denser when
254 cultured with salivary gland mesenchyme, and grew and branched at a faster rate than
255 with any of the mammary mesenchymes tested (Fig. 4a, top row). Of E13.5 mammary
256 epithelia, majority (13 out of 18) did not survive in the salivary gland mesenchyme, and in
257 the remaining ones, only traces of epithelial cells could be detected after 6 days of culture
258 (Fig. 4a, middle row). However, E13.5 mammary epithelia branched readily in combination
259 with all mammary mesenchymes (Fig. 4a, middle row), although their success rate was
260 generally lower than that of E16.5 epithelia, as also previously reported [19]. In addition, we
261 assessed the impact of mammary mesenchyme on salivary gland epithelium. Although the
262 salivary gland epithelium usually survived, further growth and branching were minimal

263 when cultured with any of the mammary mesenchymes, in stark contrast with homotypic
264 control recombinants (Fig. 4a, bottom row).

265 In principle, new branches can be generated by two different mechanisms: tip
266 clefting/bifurcation or lateral (side) branching [1, 3]. In the embryonic mammary gland, both
267 events are common [7] while the salivary gland branches by tip clefting only [32]. Recent
268 advances in imaging technologies have enabled time-lapse analysis of branching events in
269 detail prompting us to perform live imaging of salivary and mammary epithelia recombined
270 *ex vivo* with salivary gland mesenchyme (Fig. 4b, Supplementary Video 1). Images were
271 captured at 2h intervals, and branching events were traced and quantified from the time-
272 lapse videos. Nearly all salivary gland branching events occurred by tip clefting (Fig. 4c),
273 as expected. Surprisingly, over 60% of mammary branching events were generated by
274 lateral branching, similar to normal embryonic mammary gland branching [7]. We conclude
275 that although salivary gland mesenchyme boosts growth of the mammary epithelium, the
276 mode of branching is an intrinsic property of the mammary epithelium that is not altered by
277 the growth-promoting salivary gland mesenchyme environment.

278 **Transcriptomic profiling of mammary and salivary gland mesenchymes identifies**
279 **potential growth regulators**

280 To identify the mesenchymal cues governing the differential growth characteristics
281 of mammary and salivary gland epithelia, we performed transcriptomic profiling of five
282 distinct tissues: E13.5 mammary mesenchyme surrounding the quiescent bud (E13.5 MM),
283 E16.5 mammary mesenchyme surrounding the mammary sprout (E16.5 MM), E16.5 Fat
284 pad precursor tissue (E16.5 FP), and E13.5 salivary gland mesenchyme (E13.5 SM) (Fig.
285 5a). E13.5 non-mammary ventral skin mesenchyme (E13.5 VM) was also included to allow
286 identification of mammary-specific transcriptomes. Five biological replicates for each tissue
287 were sequenced.

288 The principal component analysis revealed that each group of samples were distinct
289 from each other, although the E13.5 MM and E13.5 VM group quite close together
290 (Supplementary Fig. 4a). To investigate the differences between the samples and assess
291 the quality of the data, we performed pairwise comparisons and identified 51, 10, 54, 195,
292 and 393 signature genes preferentially expressed in only one of the five sample sets (Fig.
293 5b and Supplementary Table 1). Among them, *Esr1* and *Ar* encoding estrogen and
294 androgen receptors, respectively, were markers of E16.5 MM, while E16.5 FP was rich
295 with adipogenesis markers such as *Aoc3*, *Adipoq*, *Cebpa*, *Fabp4, Lpl, Plin1 and Pparg* [33].
296 E13.5 SM-enriched genes *Nr5a2*, *Negr1*, *Klf14* and *Satb2* have been identified as salivary
297 mesenchyme markers by Sekiguchi et al. using single-cell RNA sequencing [34]. These data
298 indicate that our RNAseq data represent well the transcriptomes of the designated tissues.

299 To understand the functional disparity between salivary and mammary
300 mesenchymes in promoting epithelial growth and branching, we performed a Gene
301 Ontology (GO) enrichment analysis for differentially expressed genes (DEGs) in Biological
302 Processes (BP) (Fig. 5c,d). In total, 461 GOBP terms were shared among E13.5 MM,
303 E16.5 MM and E16.5 FP when compared to E13.5 SM. Among the 461 shared GOBP
304 terms, the top 10 most significantly enriched terms in each pairwise comparison resulted
305 only into 16 unique GOBP terms. Strikingly, of these, four were Wnt pathway related
306 terms: canonical Wnt signaling pathway, regulation of canonical Wnt signaling pathway,
307 negative regulation of Wnt signaling pathway, and negative regulation of canonical Wnt
308 signaling pathway (Fig. 5d).

309 To identify genes with the potential to regulate epithelial cell behaviors, we focused
310 on DEGs encoding extracellular (secreted or membrane-bound) molecules (signaling
311 molecules, signaling pathway inhibitors, extracellular matrix components) in biologically
312 relevant pairwise comparisons (Fig. 5e). Exclusion of lowly expressed genes led to the

313 identification of 644 candidate genes (Supplementary Table 2). mFuzz cluster analysis [35]
314 suggested that those genes could be further classified into 9 clusters based on their
315 expression pattern across all the samples (Fig. 5f and Supplementary Table 2).
316 Examination of the Wnt pathway related genes (as identified by GOBP enrichment
317 analysis shown in Fig. 5d) in these clusters revealed that altogether 12 out of 19 negative
318 regulators of Wnt pathway were markers of clusters 1 and 3, including *Dkk2*, *Bmp2*,
319 *Wnt11*, *Slc9a3r1*, *Grem1*, *Wif1*, *Tsku*, *Wnt5a*, *Dkk1*, *Notum*, *Sostdc1* and *Cthrc1* (Fig. 5g).
320 Clusters 1 and 3 were characterized by genes displaying lower expression in E16.5 MM
321 than E13.5 MM, and the lowest level in E13.5 SM (Fig. 5f). Our tissue recombination
322 experiments (Fig. 1b) suggest that such an expression pattern might represent potential
323 growth suppressors. In other words, low expression of these negative regulators in salivary
324 gland mesenchyme might enhance epithelial growth and branching, and in turn their
325 higher expression in mammary mesenchyme might inhibit growth.
326 Clusters 2, 7, 8 and 9 were defined by genes such as *Hgf*, *Ltbp1, Tnc, and Postn,*
327 with highest expression levels in one or more mammary-derived mesenchymes,
328 highlighting them as best candidates to possess mammary-specific functions, e.g. in
329 regulation of sprouting or epithelial cell differentiation. On the other hand, the clusters 5
330 and 6 genes, such as *Adam10*, *Adamts1*, *Bmp1*, *Bmp7*, *Fgf10*, *Igf1*, *Igf2* and *Eda,* have
331 highest expression levels in E13.5 SM, indicating a potential role as drivers of epithelial
332 growth. This fits well with the known roles of Eda and Fgf10 in salivary and mammary
333 gland development [7, 13, 36-38].

334 **Wnt-activated mesenchyme promotes growth of the mammary epithelium**

335 The transcriptomic analysis suggests that one significant difference between salivary
336 and mammary mesenchymes is the Wnt pathway. Gene set variation analysis (GSVA)
337 confirmed that the Wnt signaling signature was higher in E13.5 SM compared to all

338 mammary mesenchymes (Supplementary Fig. 4b), which is consistent with the high
339 expression of Wnt inhibitors in the mammary mesenchyme. Moreover, we have previously
340 shown that suppression of mesenchymal Wnt activity in developing salivary glands
341 compromises growth of the salivary gland [36]. Together, these findings promoted us to ask
342 whether low levels of mesenchymal Wnt activity could limit the growth of the mammary
343 epithelium. To answer this question experimentally, we aimed to activate Wnt signaling by
344 stabilizing β-catenin in the mesenchyme by crossing *Dermo1-Cre*$^{+/-}$ mice with those
345 harboring exon3 –floxed ß-catenin (*ß-catenin*$^{flox3/flox3}$ mouse) [39]. However, this led to
346 embryonic lethality already at E12.5, in line with previous reports [40]. Therefore, we chose
347 the tissue recombination approach where E13.5 wild type mammary buds were
348 recombined with E13.5 mammary mesenchyme dissected either from control (*ß-*
349 *catenin*$^{wt/wt}$) or *ß-catenin*$^{flox3/wt}$ embryos, followed by adeno-associated virus (AAV8) –
350 mediated gene transduction as a means to deliver Cre recombinase [41] (Fig. 6a). As a
351 result, Wnt signaling was activated in the mesenchymal cells only. Quantification of tissue
352 recombinants transduced with AAV8-Cre revealed that wild type mammary epithelia
353 cultured on mammary mesenchyme from *ß-catenin*$^{flox3/wt}$ embryos had significantly more
354 ductal tips than those cultured on control mammary mesenchyme (Fig 6b,c). These data
355 indicate that low level of mesenchymal Wnt signaling activity limits growth and branching
356 of the mammary epithelium.

357 Next, we asked which paracrine factors could regulate epithelial growth downstream of
358 mesenchymal Wnt signaling. First, we explored a publicly available RNA-seq dataset [42]
359 (Fig. 6d) which compared gene expression levels in wild type and β-catenin deficient
360 mammary fibroblasts cultured with or without Wnt3a protein, and narrowed our analysis on
361 cluster 5 and 6 genes identified in the mFuzz analysis (Fig. 5f and Supplementary Table
362 2). These genes displayed opposite expression patterns to genes in clusters 1 and 3, and

363 hence were expected to positively regulate epithelial growth (Fig. 5f,g). The analysis
364 revealed that the expression of most of the cluster 5 and 6 genes was altered in mammary
365 fibroblasts upon manipulation of Wnt signaling activity (Fig. 6d). Focusing on genes
366 upregulated by Wnt3a in wild type, but not in β-catenin deficient fibroblast led to the
367 identification of 18 and 5 candidate genes in clusters 5 and 6, respectively, *Eda* and *Igf1*
368 being amongst them (Fig. 6d-f). We have previously identified *Eda* as a gene downstream
369 of Wnt pathway in the salivary gland mesenchyme [36], validating our analysis pipeline.

370 **IGF-1R is required for embryonic mammary gland development and branching**
371 **morphogenesis**

372 IGF-1 is well known for its role in growth control and, similar to other tissues, it
373 functions as an important local mediator of the growth hormone in pubertal mammary
374 glands [43-45]. However, the role of the IGF-1 pathway in embryonic mammary gland
375 development has not been explored, apart from one study reporting the smaller size of the
376 E14 mammary bud in IGF-1R deficient embryos [46]. Analyses of the known secreted
377 components of the IGF pathway revealed that many of them were differentially expressed
378 between salivary and mammary gland mesenchymes (Supplementary Fig. 5), the most
379 striking being *Igf1* and pregnancy-associated plasma protein-A (*Pappa*), a zinc
380 metalloproteinase that promotes IGF-1 signaling through cleavage of the inhibitory Igf-
381 binding proteins (IGFBPs) [47]. *Pappa* was also identified as a cluster 5 gene in the mFuzz
382 analysis (Supplementary Table 2). To functionally test the effect of IGF-1 on mammary
383 gland growth, we performed *ex vivo* culture of E16.5 mammary glands and treated the
384 explants for 3 days with moderate levels of recombinant IGF-1 or vehicle (Fig. 7a).
385 Quantification of branch tip number showed that IGF-1 significantly increased growth of
386 the mammary epithelium (Fig. 7b).

387 To assess the function of IGF-1 *in vivo*, we examined mammary gland development in
388 embryos deficient for *Igf1r*, the obligate cognate receptor of Igf1 [48, 49]. As previously
389 reported [50], *Igf1r*$^{-/-}$ embryos were significantly smaller compared with wild type littermates
390 (*Igf1r*$^{+/+}$) (Fig. 7c). At E16.5, the anterior glands of littermate control embryos had sprouted.
391 Small outgrowths were also observed in *Igf1r*$^{-/-}$ embryos, with the exception of mammary
392 gland 3 that was consistently absent (Fig. 7d). At E18.5, growth and branching was
393 severely compromised in the *Igf1r*$^{-/-}$ embryos, verified by quantification of the epithelial
394 area of the mammary gland and the ductal tip number of mammary glands 1-4 at E18.5
395 (Supplementary Fig. 6a,b). To avoid biases caused by the conspicuously smaller size of
396 the *Igf1r*$^{-/-}$ embryos [50, 51], we normalized the data to the body weight (Fig. 7e,f). The
397 normalized values revealed that the mammary gland area and tip numbers were
398 significantly reduced in *Igf1r*$^{-/-}$ embryos compared to controls. There was no significant
399 difference between *Igf1r*$^{+/-}$ and *Igfr1*$^{+/+}$ embryos, except that the number of tips in mammary
400 gland 2 was reduced in *Igf1r*$^{+/-}$ embryos (Fig. 7f). Analysis of E13.5 embryos revealed that
401 mammary rudiment 3 was absent in *Igf1r*$^{-/-}$ embryos already early on (Supplementary Fig.
402 6c,d). We also examined the developing salivary glands at E13.5, E16.5 and E18.5. In
403 stark contrast to the mammary gland, the salivary glands of E16.5 and E18.5 *Igf1r*$^{-/-}$
404 embryos were highly branched although smaller (Supplementary Fig. 6e), paralleling the
405 overall growth defect of the mutant embryos (Fig. 7c). Collectively, these data show that
406 embryonic mammary gland development is exceptionally sensitive to loss of IGF-1/IGF-1R
407 signaling, as shown by the complete absence of mammary bud 3 and the specific growth
408 and branching impairment during late embryogenesis.
409
410 **Discussion**

411 In this study, we explored the fundamental principles of epithelial-mesenchymal
412 tissue interactions guiding embryonic mammary gland development. Our findings reveal
413 that while both the timing and type of branching events are intrinsic properties of the
414 mammary epithelium, mammary-specific mesenchymal signals are crucial for the
415 acquisition of the branching capacity. Importantly, we demonstrate that salivary gland
416 mesenchyme could only promote the growth of mammary epithelium without changing the
417 branching regime. Transcriptomic profiling and experimental evidence indicate that
418 mesenchymal Wnt signaling and Igf1 downstream of it are critical regulators promoting
419 mammary gland growth and contribute to the differences in growth-promoting capacity of
420 the mammary and salivary mesenchymes. Other pathways are also involved, as several
421 signaling molecules known to regulate growth, such as *Eda* and *Fgf10* [7, 52, 53], were
422 differentially expressed between salivary and mammary gland mesenchymes.
423 Three important events occur before initiation of mammary gland branching: exit
424 from quiescence, lineage segregation and initial outgrowth. Our data suggest that these
425 three phenomena are likely coordinated, in part through Eda signaling. Interestingly, basal
426 cells are more proliferative initially, unlike during later embryogenesis when branching is
427 ongoing [54]. Our observation that basal cell-biased proliferation is activated prior to
428 branching seems to support the previous hypothesis that proliferation and lineage
429 segregation may be prerequisites for branching [8, 10]. However, basal cells are more
430 proliferative also in K14-*Eda* mammary glands where establishment of luminal fate is
431 temporarily disrupted when branching begins. This finding argues that lineage segregation
432 is independent of onset of branching. Moreover, analyses in both Eda loss- and gain-of-
433 function mice imply that even though cell proliferation precedes, it alone is not sufficient to
434 induce branching. This is in line with our recent study showing that inhibition of cell
435 proliferation does not prevent branch point generation or branch elongation *per se*, though

436 new cells are evidently needed as building blocks for further ductal growth [54]. Instead, cell
437 motility is critical for branch point formation in the mammary gland [54], as well as in other
438 branching organs [55-57].

439 Epithelial-mesenchymal tissue recombination experiments performed mainly in the
440 50's to 70's using different branched organs, including the lung, kidney, and salivary gland,
441 have disclosed the dominant role of the mesenchyme in branch patterning [17, 58-64], a
442 conclusion confirmed also by detailed branch pattern analyses of heterotypic kidney and
443 lung tissue [18]. Similarly, recombination experiments between mammary epithelium and
444 salivary gland mesenchyme [19, 20] laid the foundation for our current understanding on the
445 instructive role of the mesenchyme in mammary gland branching morphogenesis.
446 However, at the time, time-lapse imaging was not feasible precluding a comprehensive
447 investigation of the dynamic branching process. Advances in imaging may explain our
448 contrasting result. That is, our data clearly demonstrate that although the density and
449 growth rate of the mammary ductal tree were greatly enhanced by the salivary gland
450 mesenchyme, the type of branch point formation was not. This observation suggests that
451 mammary epithelium itself carries the instructions dictating the mode of branching
452 involving both lateral branching and tip bifurcations. This conclusion is further supported by
453 our recent study showing that isolated E16.5 mammary epithelia retain bimodal branching
454 also in the mesenchyme-free 3D organoid culture [54]. Evidently, further studies are required
455 to elucidate which properties of the mammary epithelium enable its bimodal branching
456 behavior.

457 In contrast to the mode of branching, growth rate and density of the mammary
458 ductal tree was grossly altered by the salivary gland mesenchyme implying an important
459 role for paracrine factors in these processes. This, together with the failure of the salivary
460 epithelium to grow in mammary gland mesenchyme indicate that the mammary gland

461 mesenchyme is either poor in growth-promoting cues and/or rich in growth-inhibitory cues.
462 Our transcriptomic profiling suggest that it may be both. Our RNA-seq data indicated that
463 low level of mesenchymal Wnt activity may restrict mammary gland growth. Mesenchymal
464 Wnt activity is critical for the early specification of the mammary mesenchyme [65], but its
465 function beyond the bud stage is largely unknown. Here, our experimental data revealed
466 that growth and branching of the mammary gland was enhanced by mesenchymal
467 activation of Wnt/β-catenin signaling activity. Previous studies have shown that an excess
468 of Wnt ligands promotes growth of the embryonic mammary epithelium but the primary
469 target tissue was unknown [13, 66]. Our results suggest that this could be (in part) an indirect
470 effect, due to augmented mesenchymal Wnt signaling activity.

471 The IGF-1/IGF-1R signaling pathway has a critical role in the coordinate regulation
472 of body growth downstream of the pituitary growth hormone [49, 67]. In its absence, the size
473 of the organs is also proportionally reduced [49, 68]. Here we show that the embryonic
474 mammary gland is particularly sensitive to *Igf1r* deficiency, mammary gland 3 failing to
475 develop at all. These data suggest that the role of IGF-1R during mammary gland
476 development, particularly in the branching morphogenesis, extends beyond its general
477 growth promoting function during embryonic development. The reason for this is currently
478 unknown but one possibility is that the availability of active IGFs in mammary gland
479 mesenchyme is limited to begin with, due to low expression of *Pappa*. Normally, the IGFs
480 exist in the form of binary complexes with IGFBPs, and PAPPA degrades IGFBPs,
481 increasing the bioavailable fraction of IGFs thereby promoting activation of IGF-1R [49].

482 In conclusion, our findings provide valuable insights into the growth control of the
483 mammary gland and the transcriptomic profiling of different mesenchymes as a novel
484 resource for investigating the mesenchymal contribution in organ development.
485 Intriguingly, we found that heterochronic mammary mesenchyme did not advance/delay

486 the timing of epithelial outgrowth and branching, indicating that mechanisms intrinsic to the
487 mammary epithelium govern these processes. Yet, mammary-specific mesenchyme was
488 indispensable for branching to occur, suggesting that mammary mesenchyme may provide
489 permissive cues that allow the mammary bud to exit quiescence and become competent to
490 respond to mitogenic cues. Parathyroid hormone like hormone (Pthlh, also known as
491 Pthrp) signaling may play a critical role here: deletion of the mesenchymally expressed
492 receptor *Pthr1* or the epithelially expressed ligand halts mammary gland development at
493 E15.5-E16.5, prior to onset of branching [69]. However, the downstream targets of Pthr1 are
494 incompletely understood, but both Wnt and bone morphogenetic protein (Bmp) pathways
495 are involved [65, 70]. In addition, the transcriptomic and epigenetic changes taking place in
496 the mammary epithelium between the quiescent bud stage and growth competent sprout
497 are currently unknown. Uncovering how mammary epithelial cells acquire their remarkable
498 growth potential and identification of the underlying mesenchymal cues are fascinating
499 avenues for future research with implications to our understanding of basic breast biology,
500 as well as breast cancer.
501

502 # Methods

503 ## Mice

504 To obtain mice constitutively expressing the Fucci2a cell cycle reporters (R26R-
505 Fucci2a-del/del), the conditional R26R-Fucci2a-floxed/floxed (Fucci2a$^{floxed/floxed}$) mice [25]
506 were first bred with PGK-Cre mice [71] ubiquitously expressing Cre. The obtained PGK-
507 Cre;Fucci2a$^{del/floxed}$ offspring were used to generate Fucci2a (R26R-Fucci2a-del/del) mice
508 without the PGK-Cre transgene. Heterozygous R26R-Fucci2a-del/wt embryos were used
509 for the quantitative analysis. The dual fluorescent mGFP;mTmG (R26-mGFP;mTmG) mice
510 were generated by breeding mTmG (R26R-mTmG/mTmG) mice (ICR background; the
511 Jackson Laboratory Stock no. 007576) with mGFP (R26R-mGFP/wt) mice (mixed
512 background). The mGFP allele was generated by breeding mTmG mice with PGK-Cre
513 mice [71] to remove the sequence containing the mTdtomato coding region and STOP
514 cassette surrounded by loxP sites leading to ubiquitous expression of mGFP. The
515 obtained PGK-Cre;mGFP mouse was bred with wild type C57Bl/6 mouse to remove the
516 PGK-Cre transgene. For embryonic tissue recombination experiments, male mGFP;mTmG
517 mice were mated with wild type NMRI females. K14-*Eda* and *Eda*$^{-/-}$ mice were maintained
518 as described previously [13]. The K14-*Eda*;Fucci2a embryos were obtained by crossing K14-
519 *Eda* males with Fucci2a-del/del females. As the *Eda* gene is localized in the X-
520 chromosome, to obtain the Fucci2a;*Eda*$^{-/-}$ and Fucci2a;*Eda*$^{+/+}$ embryos, the Fucci2a mice
521 were first bred with *Eda*$^{-/y}$ male or *Eda*$^{-/-}$ female to obtain Fucci2a;*Eda*$^{+/y}$ and Fucci2a;*Eda*$^{-/y}$
522 males, and Fucci2a;*Eda*$^{+/-}$ females. For the analysis, the Fucci2a;*Eda*$^{-/-}$ embryos were
523 obtained by breeding Fucci2a;*Eda*$^{-/y}$ males with Fucci2a;*Eda*$^{+/-}$ females and Fucci2a;*Eda*$^{+/+}$
524 embryos were obtained by breeding Fucci2a;*Eda*$^{+/y}$ males with Fucci2a;*Eda*$^{+/-}$ females.
525 The *ß-catenin*$^{flox3/flox3}$ mice [39] were maintained in C57Bl/6 background as described
526 previously [72]. *ß-catenin*$^{flox3/flox3}$ or *ß-catenin*$^{wt/wt}$ (wild type C57Bl/6) male mice were bred

527 with C57Bl/6 wild type females to obtain the *ß-catenin*$^{flox3/wt}$ or *ß-catenin*$^{wt/wt}$ embryos for
528 the AAV virus transduction experiments. *Igf1r*$^{+/-}$ mice were maintained in 129S2/SvPasCrl
529 background as described previously [51]. The littermates obtained from breeding of *Igf1r*$^{+/-}$
530 male and *Igf1r*$^{+/-}$ female mice were used for analysis.
531 All mice were kept in 12 hours light-dark cycles with food and water given ad
532 libitum. The appearance of the vaginal plug was considered as embryonic day 0.5, and the
533 age of the embryos was further verified based on the limb and craniofacial morphology
534 and other external criteria [73]. For embryos older than E13.5, only female embryos were
535 used for experiments and analysis. The gender was determined by the morphology of the
536 gonad as described previously [21] and further confirmed by detecting the Y chromosomal
537 *Sry* gene using PCR [74].
538
539 ***Ex vivo* embryonic tissue culture and tissue recombination**
540 *Ex vivo* culture of embryonic mammary glands was performed as described earlier
541 [21]. Briefly, the abdominal-thoracic skin containing mammary glands 1-3 was dissected from
542 E13.5 to E16.5 embryos. The tissues were treated for 30-60 min with 2.5 U/ml of Dispase
543 II (4942078001; Sigma Aldrich) in PBS at +4ºC in the shaker and then 3-4 min with a
544 pancreatin-trypsin (2.5 mg/ml pancreatin [P3292; Sigma Aldrich] and 22.5 mg/ml trypsin
545 dissolved in Thyrode´s solution pH 7.4) at room temperature. The tissues were incubated
546 in culture media (10% FBS in 1:1 DMEM/F12 supplemented with 100 µg/ml ascorbic acid,
547 10 U/ml penicillin and 10 mg/ml streptomycin) on ice for a minimum of 30 min before
548 further processing. The skin epithelium was removed with 26-gauge needles leaving the
549 mesenchymal tissue with the mammary buds.
550 For typical mammary gland culture, the tissues were collected on small pieces of
551 Nuclepore polycarbonate filter with 0.1 µm pore size (WHA110605, Whatman) and further

552 cultured on the air-liquid interface on filters with the support of metal grids in a 3.5 cm
553 plastic Petri dish with culture medium. The explants were cultured in a humidified incubator
554 at 37°C with an atmosphere of 5% CO_2 and the culture medium was replaced every other
555 day.

556 To test the role of Igf1 in branching morphogenesis, recombinant mouse IGF1
557 protein (791-MG, R&D systems) at the final concentration of 150 ng/ml was added to the
558 culture medium 3 hours after the onset of the culture. The same volume of 10% BSA was
559 used as a vehicle control. The fresh culture medium with IGF1 or BSA was replaced after
560 two days, and the explants were cultured for three days in total.

561 For tissue recombination experiments, embryos expressing mGFP or mTmG were
562 identified with a fluorescent stereomicroscope and processed separately. The E13.5
563 submandibular glands (hereafter salivary gland) were dissected and processed similarly as
564 described above for the mammary gland. After enzyme treatment and incubation on ice,
565 the tissues were further dissected under a stereomicroscope to separate the intact
566 mammary or salivary gland epithelium and their mesenchyme. The mesenchymes without
567 any epithelium were collected with the filter and maintained in the culture incubator until
568 further use. For salivary mesenchyme, mesenchymes from 3-4 salivary glands were
569 pooled into one piece of filter to increase the amount of mesenchyme in each sample.
570 After epithelial-mesenchymal separation of all samples, salivary epithelium or mammary
571 buds 1-3 were gently washed by pipetting through a 1000 μl tip several times to remove
572 the remaining mesenchymal tissues and then transferred onto the mesenchyme
573 expressing different fluorescent protein, as previously described [41]. 1-2 mammary buds
574 were transferred to each mesenchyme. The recombinants were cultured as described
575 above.

576 To specifically activate the WNT/ß-catenin signaling in the mesenchyme, tissue
577 recombination has been performed as described above, while the mesenchymes from
578 E13.5 *ß-catenin*$^{flox3/wt}$ or *ß-catenin*$^{wt/wt}$ embryos were recombined with mammary buds from
579 *ß-catenin* $^{wt/wt}$ embryos. 2 hours after culture, final concentration of 1.13x10^{7} vg/µl AAV8-
580 Cre (purchased from AAV Gene Transfer and Cell Therapy Core Facility, Faculty of
581 Medicine, University of Helsinki) were added into the culture medium. The fresh culture
582 medium without virus was replaced every other day, and the explants were cultured 6-7
583 days in total.
584
585 **Time-lapse imaging for recombinants**
586 To monitor the growth of the recombinants, the explants were imaged with Zeiss
587 Lumar microscope equipped with Apolumar S 1.2x objective once per day. To assess the
588 branching type of each event of the epithelium in salivary mesenchyme, multi-position,
589 automated time-lapse imaging described previously [21] was used instead. Briefly, tissue
590 recombination was performed as described above (Day 0). 1-2 days after the culture,
591 explants with filter were transformed to 24 mm Transwell inserts with 0.4 µm polyester
592 membrane (CLS3450, Costar) and cultured on 6-well plates allowing multi-position
593 imaging [7]. From day 1 or 2 to day 4 of culture, explants were imaged with 3i Marianas
594 widefield microscope equipped with 10x/0.30 EC Plan-Neofluar Ph1 WD=5.2 M27 at 37 °C
595 with 6% CO2. The medium was changed right before the imaging and thereafter, every
596 other day. Images were acquired with an LED light source (CoolLED pE2 with 490 nm/550
597 nm) every 2 hours.
598
599 **Mesenchyme-free mammary rudiment culture and time-lapse imaging**

600 E13.5 to E16.5 mammary rudiments were cultured in 3D Matrigel as previously
601 described [21]. Briefly, after separation of the mammary tissue with mesenchyme, the intact
602 mammary rudiments 1-3 were dissected under stereomicroscope as described above. The
603 mammary rudiments collected from littermate embryos of same genotype were pooled
604 together, except for *Eda*$^{-/-}$ or *Eda*$^{+/+}$. Pooled mammary rudiments 1-3 from each *Eda*$^{-/-}$ and
605 *Eda*$^{+/+}$ embryo were cultured separately as it is not possible to obtain *Eda*$^{-/-}$ and *Eda*$^{+/+}$
606 genotypes from the same litter. Intact mammary rudiments were transferred onto the
607 bottom of 12-well plates with 10 µl of culture media. The medium was then replaced with a
608 20-30 µl drop of growth-factor reduced Matrigel (356231; Corning) using a chilled pipette
609 tip. The MBs were dispersed to avoid any potential contact with each other or the bottom
610 of the plate. The mixture was then incubated in the 37°C culture incubator for 15-20
611 minutes until the matrix was solidified. The MBs were cultured in a humidified incubator at
612 37°C with an atmosphere of 5% CO_2 in serum-free DMEM/F12 medium supplemented
613 with 1X ITS Liquid Media Supplement (I3146, Sigma Aldrich] and 2.5 nM hFGF2 (CF0291;
614 Sigma Aldrich), 10 U/ml penicillin and 10 000 µg/ml streptomycin. The culture medium was
615 replaced every other day and the growth of the MBs was monitored once per day by
616 imaging with Zeiss Lumar microscope.
617
618 **Whole-mount immunofluorescence staining and imaging**
619 For whole-mount immunofluorescence staining, dissected ventral skin containing
620 mammary glands, cultured explants, or mammary epithelia cultured in Matrigel were fixed
621 in 4% PFA at 4°C overnight, washed three times in PBS and then three times in 1% PBST
622 (1% TritonX-100 in PBS) at room temperature. Samples were blocked with blocking buffer
623 containing 5% normal donkey serum, 0.5% BSA, and 10 µg/ml Hoechst 33342 (Molecular
624 Probes/Invitrogen) in 1% PBST at 4°C overnight. The samples were then incubated with

625 primary antibodies diluted in blocking buffer for 1-2 days at 4°C, washed three times with
626 0.3% PBST at room temperature before incubation with secondary antibodies diluted in
627 0.3% PBST with 0.5% BSA for 1-2 days at 4°C. After washing three times with 0.3% PBST
628 and three times with PBS, samples were post-fixed with 4% PFA for 10 minutes at room
629 temperature. Finally, samples were washed twice with PBS before immersing into the
630 fructose-glycerol based clearing solution described by Dekker et al. [75] before imaging. For
631 samples from older embryos, the blocking step was extended to 2 days followed by an
632 extra microdissection procedure, where samples were dissected under fluorescence
633 stereomicroscope to expose the mammary epithelium and remove surplus mesenchymal
634 tissues. The samples were imaged with Leica TCS SP8 inverted laser scanning confocal
635 microscope with HC PL APO 20x/0.75 IMM CORR CS2 object. The images were acquired
636 with z-stack of 0.11 µm intervals.

637 For E13.5 *Igf1r* embryos, the staining was performed with the whole embryos
638 before imaging. The samples of *Igf1r* embryos or IGF1-treated explants were imaged with
639 Lumar stereomicroscope.

640 The following antibodies were used in this study: rat anti-mouse CD326 (EpCAM,
641 552370, BD Pharmingen, 1:500), rabbit anti-mouse Krt14 (RB-9020-P, Thermo Fisher
642 Scientific, 1:500), rat anti-Krt8 (TROMA-1, DSHB, 1:500), Alexa Fluor 488-conjugated
643 Donkey anti-Rat secondary antibody (A21208, Invitrogen, 1:500) and Alexa Fluor 647-
644 conjugated Donkey anti-Rat secondary antibody (A48272, Invitrogen, 1:500).

645

646 **Image analysis**

647 For mammary gland volume quantification, the border of mammary epithelium and
648 mesenchyme was outlined manually based on EpCAM expression and bud morphology
649 and the surface rendering and volume quantification were performed with Imaris 9.2

650 software (Bitplane). The mammary gland tip number was counted manually in 3D using
651 Imaris. To further quantify the cell cycle dynamics of mammary epithelial cells, the
652 mammary epithelium was masked using the rendered mammary gland surface in Imaris.
653 Epithelial cells expressing nuclear mCherry (G1/G0) or nuclear mVenus (S/G2/M) were
654 automatically detected using spot detection function with manual correction. The distance
655 of each detected nucleus to the mammary epithelium surface was measured using the
656 distance transformation function of Imaris. All the data were exported to be further
657 analyzed using R version 4.2.1, a free software environment available at https://www.r-
658 project.org/.

659 To quantify the mammary gland growth affected by the deficient of *Igf1r,* the
660 epithelial area of the mammary glands and the number of ductal tips were acquired
661 manually with ROI Manager within ImageJ (Fiji, version 1.53t) [76]. -Time-lapse images were
662 analyzed with ImageJ manually.

663 The plots were produced with R using packages tidyverse version 1.3.2 [77], ggplot2
664 version 3.4.0 [78], ggsignif version 0.6.4 [79], ggpubr version 0.4.0 [80] and RcolorBrewer
665 version 1.1-3 [81].

666

667 **RNA sequencing and data analysis**

668 To obtain the mesenchyme samples for RNA sequencing, salivary glands or flank skins
669 with mammary rudiments 1-3 were dissected and followed by enzyme treatment as
670 described above for *ex vivo* embryonic tissue culture. E13.5 salivary gland mesenchymes
671 were obtained after removing the salivary gland epithelium. For E13.5 and E16.5
672 mammary gland mesenchymes, after removing the skin epithelium, the mammary
673 epithelium and its surrounding mesenchyme were isolated together with small scissors
674 followed by removal of the mammary epithelium using 26-gauge needles (303800, BD

675 Microlance). The E16.5 fat pad precursor was microdissected from the explants after
676 enzyme treatment. The E13.5 ventral skin mesenchymes further away from the mammary
677 gland region were collected as E13.5 skin mesenchyme. The mesenchymes isolated from
678 2-3 embryos from the same litter were pooled together as one sample. Altogether, five
679 biology replicates for each sample were collected from 3 different litters of
680 C57Bl/6JOlaHsd mice. Samples were lysed immediately after collection and stored in TRI
681 Reagent (T9424, Sigma) at -80°C. Total RNA was extracted using Direct-zol RNA
682 Microprep kit (Zymo Research, Irvine, CA) with DNase treatment according to the
683 manufacturer's instructions. RNA quality was assessed with 2100 Bioanalyzer (Agilent,
684 Santa Clara, CA) using Agilent RNA 6000 Pico Kit or Agilent RNA 6000 Nano Kit (Agilent,
685 Santa Clara, CA). RNA concentration was determined using Qubit RNA HS Assay Kit
686 (Q32855, Thermo Fisher) with Qubit 4 Fluorometer (Thermo Fisher). cDNA libraries were
687 prepared with Ovation SoLo RNA-seq System (NuGen/Tecan Genomics) according to
688 manufacturer's instructions and sequenced with NextSeq 500 (Illumina, San Diego, CA) in
689 the DNA Genomics and Sequencing core facility, Institute of Biotechnology, HiLIFE,
690 University of Helsinki. 45-68 million reads per sample were obtained after 3 rounds of
691 sequencing.

692 For RNAseq data analysis, all sequencing reads were processed for quality control,
693 removal of low-quality reads, adaptor sequence and ribosomal RNA using fastqc version
694 0.11.8 [82], multiqc version 1.9 [83], Trimmomatic version 0.39 [84] and SortMeRNA version 2.1
695 [85] accordingly. The filtered reads were mapped to the reference genome (mm10) using
696 Salmon version 0.99.0 [86] resulting in 36.6 to 53.4 million mapped reads per sample. The
697 GSVA analysis was performed with R package GSVA version 1.44.5 [87]. The conversion of
698 murine gene Ensembl IDs to human Entrez IDs was performed with the biomaRt package
699 version 2.46.3 [88, 89], using the reference mart https://dec2021.archive.ensembl.org. The

700 significant differentially expressed signatures between different mesenchymes were
701 assessed with lmFit and eBayes functions from R package limma version 3.52.4 [90], by
702 comparing E13.5 MM, E16.5 MM or E16.5 FP with E13.5 SM, respectively. The signature
703 database was downloaded from www.gsea-msigdb.org [91] on 12th February 2023. The
704 significantly enriched KEGG signaling pathways were pooled together for visualization.
705 The data normalization and analysis of differentially expressed genes (DEGs) were
706 performed using the R package DESeq2 version 3.15 [92]. DEGs were defined with the
707 thresholds of average count number > 50, adjusted p-value <0.05 and Log2(Fold
708 Change) >=0.58 in each pairwise comparison.

709 Gene Ontology enrichment analysis was performed with the DEGs using R package
710 pathfindR version 1.6.4 [93]. Only the GOBP terms with lowest adjusted p value less than
711 0.01 were considered as significant. Among the commonly significantly altered GOBP
712 terms, the top 10 GOBP terms with lowest adjusted p-value in each comparison and totally
713 16 GO terms were plotted. Gene Ontology database was downloaded from MSigDB [91]
714 using R package msigdbr version 7.5.1 [94] on 9th November 2022.

715 The DEGs with an average count number >100 and upregulated more than twice
716 (Log2(Fold change)>=1) in each group of samples compared to all the other 4 groups of
717 samples were identified as marker genes.

718 To detect the pattern of the gene expression among different mesenchymal tissues,
719 DEGs encoding extracellular matrix protein or ligands in selected pairwise comparisons
720 with an average count number >200 in each group were further analyzed using Mfuzz
721 version 2.58.0 [95]. The average of the normalized count number of each group was used as
722 input. In addition, the groups were converted to pseudotime for the analysis. The fuzzifier
723 m was determined with the default function and returned a value of 2.113207. The number
724 of clusters was optimized empirically and set as 9 for the final analysis. The curated

725 database including ECM, Ligand or Receptor genes was combined from the databases of
726 R package SingleCellSignalR version 1.2.0 [96], CellTalkDB version 1.0 [97] and curated GO
727 terms downloaded from https://baderlab.org/CellCellInteractions [98].
728 The plots were produced using R packages tidyverse version 1.3.2 [77], ggplot2
729 version 3.4.0 [78], circlize version 0.4.15 [99], RcolorBrewer version 1.1-3 [81], pathfindR version
730 1.6.4 [93], ComplexHeatmap version 2.12.1 [100], venn version 1.11 [101] and patchwork version
731 1.1.2 [102].
732
733 **Public RNAseq data analysis**
734 The raw data from Wang et al. [42] (OEP001019) were downloaded from
735 https://www.biosino.org/node/index. The sequence reads were processed similarly as
736 described above. The log2 transformed normalized expression of selected genes were
737 extracted to construct the heatmap shown in Fig. 6D.
738
739 **Statistical analysis**
740 All data were analyzed by Prism 9 (GraphPad Software), or R packages ggsignif
741 version 0.6.4 [79] and ggpubr version 0.4.0 [80]. Statistical tests used are indicated in figure
742 legends. p-values < 0.05 were considered significant. Throughout the figure legends: *p <
743 0.05, **p<0.01; ***p < 0.001, ****p < 0.0001.
744
745 **Ethics statement**
746 All mouse experiments were approved by the Laboratory Animal Center at the
747 University of Helsinki and the National Animal Experiment Board of Finland with the
748 licenses number KEK19-019, KEK22-014 and ESAVI/2363/04.10.07/2017. Mice were
749 euthanized with CO_2 followed by cervical dislocation.

750

751 **Data availability**

752 The raw and processed RNAseq data created in this study have been deposited in
753 the GEO database under the access code GSEXXXXXX.

754

755 **Code availability**

756 The code used for the analyses is open-source and available through the R
757 packages described in the methods. All the customized scripts for producing the figures in
758 this study are available upon request to the corresponding author.

759

760 **Acknowledgements**

761 The authors wish to thank Dr. Jianpin Cheng, Dr. Alison Kuony and M.Sc. Aida
762 Kaffash Hoshiar for the critical comments and suggestions on the manuscript, Ms. Raija
763 Savolainen and Ms. Merja Mäkinen for excellent technical assistance, Dr. Maria
764 Voutilainen, Dr. Satu-Marja Myllymäki and Dr. Ana-Marija Sulić for technical advice, past
765 and present members of the Mikkola lab for insightful discussions. We also acknowledge
766 Dr. Rishi Das Roy for the important discussion on RNAseq data analysis and CSC – IT
767 Center for Science, Finland, for computational resources. AAVs were provided by AAV
768 Gene Transfer and Cell Therapy Core Facility, Faculty of Medicine, University of Helsinki.
769 Confocal and widefield microscope imaging and image analysis were performed at the
770 Light Microscopy Unit, Institute of Biotechnology, supported by HiLIFE and Biocenter
771 Finland. RNA sequencing was performed in the DNA Sequencing and Genomics Unit at
772 the Institute of Biotechnology, HiLIFE, University of Helsinki. This work was carried out
773 with the support of HiLIFE Laboratory Animal Centre Core Facility, University of Helsinki,
774 Finland.

775 This work was supported by the Academy of Finland project grant (318287 to
776 M.L.M.) and Center of Excellence Program (272280 and 307421 to M.L.M.), the Cancer
777 Society of Finland (M.L.M.), the Jane and Aatos Erkko Foundation (M.L.M.), the Sigrid
778 Jusélius Foundation (M.L.M.), the HiLIFE Fellow Program (M.L.M.), Oskar Öflunds
779 Foundation (Q.L.), the Doctoral Programme in Integrative Life Science of the University of
780 Helsinki (E.T.), the Doctoral Programme in Biomedicine (M.C.), the Finnish Cultural
781 Foundation (J.S. and B.K.), and Ella and Georg Ehrnrooth Foundation (J.S.).

782

783 **Author Contributions**

784 Conceptualization, Q.L., M.L.M.; Methodology, Q.L., R.L.; Software, Q.L.; Validation,
785 Q.L.; Formal analysis, Q.L., J.S., B.K.; Investigation, Q.L., E.T., R.L., J.S., M.C.; Resources,
786 M.H., J.J., M.L.M.; Data Curation, Q.L.; Writing – original draft preparation, Q.L., M.L.M;
787 Writing – review and editing, Q.L., E.T., R.L., J.S., B.K., M.C., M.H., J.J., M.L.M;
788 Visualization, Q.L.; Supervision, M.L.M.; Project administration, Q.L., M.L.M; Funding
789 acquisition, M.L.M.

790

791 ## References

792 1. Lang, C., Conrad, L. & Iber, D. Organ-Specific Branching Morphogenesis. *Front*
793 *Cell Dev Biol* **9**, 671402 (2021).
794 2. Goodwin, K. & Nelson, C.M. Branching morphogenesis. *Development* **147** (2020).
795 3. Myllymäki, S.-M. & Mikkola, M.L. Inductive signals in branching morphogenesis –
796 lessons from mammary and salivary glands. *Curr Opin Cell Biol* **61**, 72-78 (2019).
797 4. Watson, C.J. & Khaled, W.T. Mammary development in the embryo and adult: new
798 insights into the journey of morphogenesis and commitment. *Development* **147**
799 (2020).

800 5. Spina, E. & Cowin, P. Embryonic mammary gland development. *Semin Cell Dev*
801 *Biol* **114**, 83-92 (2021).
802 6. Sakakura, T., Suzuki, Y. & Shiurba, R. Mammary Stroma in Development and
803 Carcinogenesis. *J Mammary Gland Biol* **18**, 189 197 (2013).
804 7. Lindstrom, R. *et al.* Unraveling the principles of mammary gland branching
805 morphogenesis. *bioRxiv*, 2022.2008.2023.504958 (2022).
806 8. Lilja, A.M. *et al.* Clonal analysis of Notch1-expressing cells reveals the existence of
807 unipotent stem cells that retain long-term plasticity in the embryonic mammary
808 gland. *Nat Cell Biol* **13**, 1 (2018).
809 9. Wuidart, A. *et al.* Early lineage segregation of multipotent embryonic mammary
810 gland progenitors. *Nat Cell Biol* **20**, 666-676 (2018).
811 10. Inman, J.L., Robertson, C., Mott, J.D. & Bissell, M.J. Mammary gland development:
812 cell fate specification, stem cells and the microenvironment. *Development* **142**,
813 1028-1042 (2015).
814 11. Cowin, P. & Wysolmerski, J. Molecular Mechanisms Guiding Embryonic Mammary
815 Gland Development. *Cold Spring Harbor Perspectives in Biology* **2**, a003251-
816 a003251 (2010).
817 12. Hiremath, M. & Wysolmerski, J. Parathyroid hormone-related protein specifies the
818 mammary mesenchyme and regulates embryonic mammary development. *J*
819 *Mammary Gland Biol Neoplasia* **18**, 171-177 (2013).
820 13. Voutilainen, M. *et al.* Ectodysplasin regulates hormone-independent mammary
821 ductal morphogenesis via NF-κB. *Proc National Acad Sci* **109**, 5744 5749 (2012).
822 14. Elo, T. *et al.* Ectodysplasin target gene Fgf20 regulates mammary bud growth and
823 ductal invasion and branching during puberty. *Scientific Reports* **7**, 5049-5049
824 (2017).

825 15. Chu, E.Y. *et al.* Canonical WNT signaling promotes mammary placode
826 development and is essential for initiation of mammary gland morphogenesis.
827 *Development* **131**, 4819-4829 (2004).
828 16. Mailleux, A.A. *et al.* Role of FGF10/FGFR2b signaling during mammary gland
829 development in the mouse embryo. *Development* **129**, 53-60 (2002).
830 17. Kispert, A., Vainio, S., Shen, L., Rowitch, D.H. & McMahon, A.P. Proteoglycans are
831 required for maintenance of Wnt-11 expression in the ureter tips. *Development* **122**,
832 3627-3637 (1996).
833 18. Lin, Y. *et al.* Patterning parameters associated with the branching of the ureteric
834 bud regulated by epithelial-mesenchymal interactions. *Int J Dev Biol* **47**, 3-13
835 (2003).
836 19. Kratochwil, K. Organ specificity in mesenchymal induction demonstrated in the
837 embryonic development of the mammary gland of the mouse. *Dev Biol* **20**, 46 71
838 (1969).
839 20. Sakakura, T., Nishizuka, Y. & Dawe, C.J. Mesenchyme-dependent morphogenesis
840 and epithelium-specific cytodifferentiation in mouse mammary gland. *Science* **194**,
841 1439-1441 (1976).
842 21. Lan, Q. *et al.* Protocol for Studying Embryonic Mammary Gland Branching
843 Morphogenesis Ex Vivo, in *Mammary Stem Cells: Methods and Protocols*. (ed. M.d.
844 Vivanco) 1-18 (Springer US, New York, NY; 2022).
845 22. Balinsky, B.I. On the prenatal growth of the mammary gland rudiment in the mouse.
846 *Journal of anatomy* **84**, 227 235 (1950).
847 23. Lee, M.Y. *et al.* Ectodermal influx and cell hypertrophy provide early growth for all
848 murine mammary rudiments, and are differentially regulated among them by Gli3.
849 *PLoS One* **6**, e26242 (2011).

850 24. Trela, E. *et al.* Cell influx and contractile actomyosin force drive mammary bud
851 growth and invagination. *J Cell Biol* **220** (2021).
852 25. Mort, R.L. *et al.* Fucci2a: a bicistronic cell cycle reporter that allows Cre mediated
853 tissue specific expression in mice. *Cell Cycle* **13**, 2681-2696 (2014).
854 26. Carabaña, C. *et al.* Positional cues underlie cell fate specification during branching
855 morphogenesis of the embryonic mammary epithelium. (2022).
856 27. Chang, S.H., Jobling, S., Brennan, K. & Headon, D.J. Enhanced Edar signalling has
857 pleiotropic effects on craniofacial and cutaneous glands. *PLoS One* **4**, e7591
858 (2009).
859 28. Williams, R. *et al.* Elevated EDAR signalling promotes mammary gland
860 tumourigenesis with squamous metaplasia. *Oncogene* **41**, 1040-1049 (2022).
861 29. Voutilainen, M. *et al.* Ectodysplasin/NF-κB Promotes Mammary Cell Fate via Wnt/β-
862 catenin Pathway. *Plos Genet* **11**, e1005676 (2015).
863 30. Lim, E. *et al.* Transcriptome analyses of mouse and human mammary cell
864 subpopulations reveal multiple conserved genes and pathways. *Breast Cancer Res*
865 **12**, R21 (2010).
866 31. Srivastava, A.K. *et al.* The Tabby phenotype is caused by mutation in a mouse
867 homologue of the EDA gene that reveals novel mouse and human exons and
868 encodes a protein (ectodysplasin-A) with collagenous domains. *Proc Natl Acad Sci*
869 *U S A* **94**, 13069-13074 (1997).
870 32. Wang, S., Sekiguchi, R., Daley, W.P. & Yamada, K.M. Patterned cell and matrix
871 dynamics in branching morphogenesis. *J Cell Biol* **216**, jcb.201610048 (2017).
872 33. Menssen, A. *et al.* Differential gene expression profiling of human bone marrow-
873 derived mesenchymal stem cells during adipogenic development. *BMC Genomics*
874 **12**, 461 (2011).

875 34. Sekiguchi, R., Martin, D., Genomics, Computational Biology, C. & Yamada, K.M.
876 Single-Cell RNA-seq Identifies Cell Diversity in Embryonic Salivary Glands. *J Dent*
877 *Res* **99**, 69-78 (2020).
878 35. Kumar, L. & M, E.F. Mfuzz: a software package for soft clustering of microarray
879 data. *Bioinformation* **2**, 5-7 (2007).
880 36. Haara, O. *et al.* Ectodysplasin and Wnt pathways are required for salivary gland
881 branching morphogenesis. *Development* **138**, 2681-2691 (2011).
882 37. Rivetti, S., Chen, C., Chen, C. & Bellusci, S. Fgf10/Fgfr2b Signaling in Mammary
883 Gland Development, Homeostasis, and Cancer. *Front Cell Dev Biol* **8**, 415 (2020).
884 38. Prochazkova, M., Prochazka, J., Marangoni, P. & Klein, O.D. Bones, Glands, Ears
885 and More: The Multiple Roles of FGF10 in Craniofacial Development. *Front Genet*
886 **9**, 542 (2018).
887 39. Harada, N. *et al.* Intestinal polyposis in mice with a dominant stable mutation of the
888 beta-catenin gene. *EMBO J* **18**, 5931-5942 (1999).
889 40. Tran, T.H. *et al.* Role of canonical Wnt signaling/ss-catenin via Dermo1 in cranial
890 dermal cell development. *Development* **137**, 3973-3984 (2010).
891 41. Lan, Q. & Mikkola, M.L. Protocol: Adeno-Associated Virus-Mediated Gene Transfer
892 in Ex Vivo Cultured Embryonic Mammary Gland. *J Mammary Gland Biol Neoplasia*
893 **25**, 409-416 (2020).
894 42. Wang, J. *et al.* Endothelial Wnts control mammary epithelial patterning via fibroblast
895 signaling. *Cell Rep* **34**, 108897 (2021).
896 43. Wood, T.L., Richert, M.M., Stull, M.A. & Allar, M.A. The insulin-like growth factors
897 (IGFs) and IGF binding proteins in postnatal development of murine mammary
898 glands. *J Mammary Gland Biol* **5**, 31-42 (2000).

899 44. Richards, R.G., Klotz, D.M., Walker, M.P. & DiAugustine, R.P. Mammary gland
900 branching morphogenesis is diminished in mice with a deficiency of insulin-like
901 growth factor-I (IGF-I), but not in mice with a liver-specific deletion of IGF-I.
902 *Endocrinology* **145**, 3106-3110 (2004).
903 45. Kleinberg, D.L. & Ruan, W. IGF-I, GH, and Sex Steroid Effects in Normal Mammary
904 Gland Development. *J Mammary Gland Biol* **13**, 353-360 (2008).
905 46. Heckman, B.M. *et al.* Crosstalk between the p190-B RhoGAP and IGF signaling
906 pathways is required for embryonic mammary bud development. *Dev Biol* **309**, 137-
907 149 (2007).
908 47. Conover, C.A. & Oxvig, C. PAPP-A and cancer. *J Mol Endocrinol* **61**, T1-T10
909 (2018).
910 48. Dupont, J. & Holzenberger, M. Biology of insulin-like growth factors in development.
911 *Birth Defects Res C Embryo Today* **69**, 257-271 (2003).
912 49. LeRoith, D., Holly, J.M.P. & Forbes, B.E. Insulin-like growth factors: Ligands,
913 binding proteins, and receptors. *Mol Metab* **52**, 101245 (2021).
914 50. Liu, J.P., Baker, J., Perkins, A.S., Robertson, E.J. & Efstratiadis, A. Mice carrying
915 null mutations of the genes encoding insulin-like growth factor I (Igf-1) and type 1
916 IGF receptor (Igf1r). *Cell* **75**, 59-72 (1993).
917 51. Holzenberger, M. *et al.* IGF-1 receptor regulates lifespan and resistance to oxidative
918 stress in mice. *Nature* **421**, 182-187 (2003).
919 52. Jaskoll, T. *et al.* FGF10/FGFR2b signaling plays essential roles during in vivo
920 embryonic submandibular salivary gland morphogenesis. *BMC Dev Biol* **5**, 11
921 (2005).

922 53. Lindfors, P.H., Voutilainen, M. & Mikkola, M.L. Ectodysplasin/NF-kappaB signaling
923 in embryonic mammary gland development. *J Mammary Gland Biol Neoplasia* **18**,
924 165-169 (2013).
925 54. Myllymäki, S., Kaczynska, B., Lan, Q. & Mikkola, M. Spatially coordinated cell cycle
926 activity and motility govern mammary ductal growth and tip bifurcation. *bioRxiv*,
927 2022.2008.2029.505725 (2022).
928 55. Kim, H.Y., Varner, V.D. & Nelson, C.M. Apical constriction initiates new bud
929 formation during monopodial branching of the embryonic chicken lung.
930 *Development* **140**, 3146-3155 (2013).
931 56. Nakanishi, Y. *et al.* Cell proliferation is not required for the initiation of early cleft
932 formation in mouse embryonic submandibular epithelium in vitro. *Development* **99**,
933 429-437 (1987).
934 57. Chi, X. *et al.* Ret-dependent cell rearrangements in the Wolffian duct epithelium
935 initiate ureteric bud morphogenesis. *Developmental Cell* **17**, 199-209 (2009).
936 58. Grobstein, C. Inductive Epithelio-mesenchymal Interaction in Cultured Organ
937 Rudiments of the Mouse. *Science* **118**, 52-55 (1953).
938 59. Alescio, T. & Cassini, A. Induction in vitro of tracheal buds by pulmonary
939 mesenchyme grafted on tracheal epithelium. *Journal of Experimental Zoology* **150**,
940 83-94 (1962).
941 60. Alescio, T. & Piperno, E.C. A quantitative assessment of mesenchymal contribution
942 to epithelial growth rate in mouse embryonic lung developing in vitro.
943 *Development* **17**, 213-227 (1967).
944 61. Alescio, T. & Di Michele, M. Relationship of epithelial growth to mitotic rate in
945 mouse embryonic lung developing in vitro. *Journal of Embryology and Experimental*
946 *Morphology* **19**, 227-237 (1968).

947 62. Lawson, K.A. Mesenchyme specificity in rodent salivary gland development: the
948 response of salivary epithelium to lung mesenchyme in vitro. *Development* **32**, 469-
949 493 (1974).
950 63. Lawson, K.A. Stage specificity in the mesenchyme requirement of rodent lung
951 epithelium in vitro : a matter of growth control? *Development* **74**, 183-206 (1983).
952 64. Iwai, K., Hieda, Y. & Nakanishi, Y. Effects of mesenchyme on epithelial tissue
953 architecture revealed by tissue recombination experiments between the
954 submandibular gland and lung of embryonic mice. *Development, Growth &*
955 *Differentiation* **40**, 327-334 (1998).
956 65. Hiremath, M. *et al.* Parathyroid hormone-related protein activates Wnt signaling to
957 specify the embryonic mammary mesenchyme. *Development* **139**, 4239-4249
958 (2012).
959 66. Cunha, G.R. & Hom, Y.K. Role of mesenchymal-epithelial interactions in mammary
960 gland development. *J Mammary Gland Biol Neoplasia* **1**, 21-35 (1996).
961 67. Streck, R.D., Wood, T.L., Hsu, M.S. & Pintar, J.E. Insulin-like growth factor I and II
962 and insulin-like growth factor binding protein-2 RNAs are expressed in adjacent
963 tissues within rat embryonic and fetal limbs. *Dev Biol* **151**, 586-596 (1992).
964 68. Powell-Braxton, L. *et al.* IGF-I is required for normal embryonic growth in mice.
965 *Genes Dev* **7**, 2609-2617 (1993).
966 69. Wysolmerski, J.J. *et al.* Rescue of the parathyroid hormone-related protein
967 knockout mouse demonstrates that parathyroid hormone-related protein is essential
968 for mammary gland development. *Development* **125**, 1285-1294 (1998).
969 70. Hens, J.R. *et al.* BMP4 and PTHrP interact to stimulate ductal outgrowth during
970 embryonic mammary development and to inhibit hair follicle induction. *Development*
971 **134**, 1221-1230 (2007).

972 71. Lallemand, Y., Luria, V., Haffner-Krausz, R. & Lonai, P. Maternally expressed PGK-
973 Cre transgene as a tool for early and uniform activation of the Cre site-specific
974 recombinase. *Transgenic Res* **7**, 105-112 (1998).
975 72. Narhi, K. *et al.* Sostdc1 defines the size and number of skin appendage placodes.
976 *Dev Biol* **364**, 149-161 (2012).
977 73. Martin, P. Tissue patterning in the developing mouse limb. *Int J Dev Biol* **34**, 323-
978 336 (1990).
979 74. Settin, A., Elsobky, E., Hammad, A. & Al-Erany, A. Rapid sex determination using
980 PCR technique compared to classic cytogenetics. *Int J Health Sci (Qassim)* **2**, 49-
981 52 (2008).
982 75. Dekkers, J.F. *et al.* High-resolution 3D imaging of fixed and cleared organoids. *Nat*
983 *Protoc* **14**, 1756-1771 (2019).
984 76. Schindelin, J. *et al.* Fiji: an open-source platform for biological-image analysis. *Nat*
985 *Methods* **9**, 676-682 (2012).
986 77. Wickham, H. *et al.* Welcome to the “tidyverse”. *Journal of Open Source Software* **4**,
987 1686 (2019).
988 78. Wickham, H. *ggplot2: Elegant graphics for data analysis*. (Springer-Verlag New
989 York, 2016).
990 79. Constantin, A.-E. & Patil, I. ggsignif: R package for displaying significance brackets
991 for 'ggplot2'. *PsyArxiv* (2021).
992 80. Kassambara, A. ggpubr: 'ggplot2' based publication ready plots. R package
993 version 0.6.0, https://CRAN.R-project.org/package=ggpubr (2023).
994 81. Neuwirth, E. RColorBrewer: ColorBrewer palettes. R package version 1.1-3,
995 https://CRAN.R-project.org/package=RColorBrewer (2022).

996 82. Andrews, S. FastQC: A Quality Control Tool for High Throughput Sequence Data.
997 http://www.bioinformatics.babraham.ac.uk/projects/fastqc/ (2010).
998 83. Ewels, P., Magnusson, M., Lundin, S. & Kaller, M. MultiQC: summarize analysis
999 results for multiple tools and samples in a single report. *Bioinformatics* **32**, 3047-
1000 3048 (2016).
1001 84. Bolger, A.M., Lohse, M. & Usadel, B. Trimmomatic: a flexible trimmer for Illumina
1002 sequence data. *Bioinformatics* **30**, 2114-2120 (2014).
1003 85. Kopylova, E., Noe, L. & Touzet, H. SortMeRNA: fast and accurate filtering of
1004 ribosomal RNAs in metatranscriptomic data. *Bioinformatics* **28**, 3211-3217 (2012).
1005 86. Patro, R., Duggal, G., Love, M.I., Irizarry, R.A. & Kingsford, C. Salmon provides fast
1006 and bias-aware quantification of transcript expression. *Nat Methods* **14**, 417-419
1007 (2017).
1008 87. Hanzelmann, S., Castelo, R. & Guinney, J. GSVA: gene set variation analysis for
1009 microarray and RNA-seq data. *BMC Bioinformatics* **14**, 7 (2013).
1010 88. Durinck, S. *et al.* BioMart and Bioconductor: a powerful link between biological
1011 databases and microarray data analysis. *Bioinformatics* **21**, 3439-3440 (2005).
1012 89. Durinck, S., Spellman, P.T., Birney, E. & Huber, W. Mapping identifiers for the
1013 integration of genomic datasets with the R/Bioconductor package biomaRt. *Nat*
1014 *Protoc* **4**, 1184-1191 (2009).
1015 90. Ritchie, M.E. *et al.* limma powers differential expression analyses for RNA-
1016 sequencing and microarray studies. *Nucleic Acids Res* **43**, e47 (2015).
1017 91. Subramanian, A. *et al.* Gene set enrichment analysis: a knowledge-based approach
1018 for interpreting genome-wide expression profiles. *Proc Natl Acad Sci U S A* **102**,
1019 15545-15550 (2005).

1020 92. Love, M.I., Huber, W. & Anders, S. Moderated estimation of fold change and
1021 dispersion for RNA-seq data with DESeq2. *Genome Biol* **15**, 550 (2014).
1022 93. Ulgen, E., Ozisik, O. & Sezerman, O.U. pathfindR: An R Package for
1023 Comprehensive Identification of Enriched Pathways in Omics Data Through Active
1024 Subnetworks. *Front Genet* **10**, 858 (2019).
1025 94. Dolgalev, I. msigdbr: MSigDB gene sets for multiple organisms in a tidy data
1026 format. R package version 7.5.1, https://CRAN.R-project.org/package=msigdbr
1027 (2022).
1028 95. Futschik, M.E. & Carlisle, B. Noise-robust soft clustering of gene expression time-
1029 course data. *J Bioinform Comput Biol* **3**, 965-988 (2005).
1030 96. Cabello-Aguilar, S. & Colinge, J. (2022).
1031 97. Shao, X. *et al.* CellTalkDB: a manually curated database of ligand-receptor
1032 interactions in humans and mice. *Brief Bioinform* **22** (2021).
1033 98. Qiao, W. *et al.* Intercellular network structure and regulatory motifs in the human
1034 hematopoietic system. *Mol Syst Biol* **10**, 741 (2014).
1035 99. Gu, Z., Gu, L., Eils, R., Schlesner, M. & Brors, B. circlize Implements and enhances
1036 circular visualization in R. *Bioinformatics* **30**, 2811-2812 (2014).
1037 100. Gu, Z., Eils, R. & Schlesner, M. Complex heatmaps reveal patterns and correlations
1038 in multidimensional genomic data. *Bioinformatics* **32**, 2847-2849 (2016).
1039 101. Dusa, A. venn: Draw venn diagrams. R package version 1.11, https://CRAN.R-
1040 project.org/package=venn (2022).
1041 102. Pedersen, T.L. patchwork: The composer of plots. R package version 1.1.2,
1042 https://CRAN.R-project.org/package=patchwork (2022).
1043

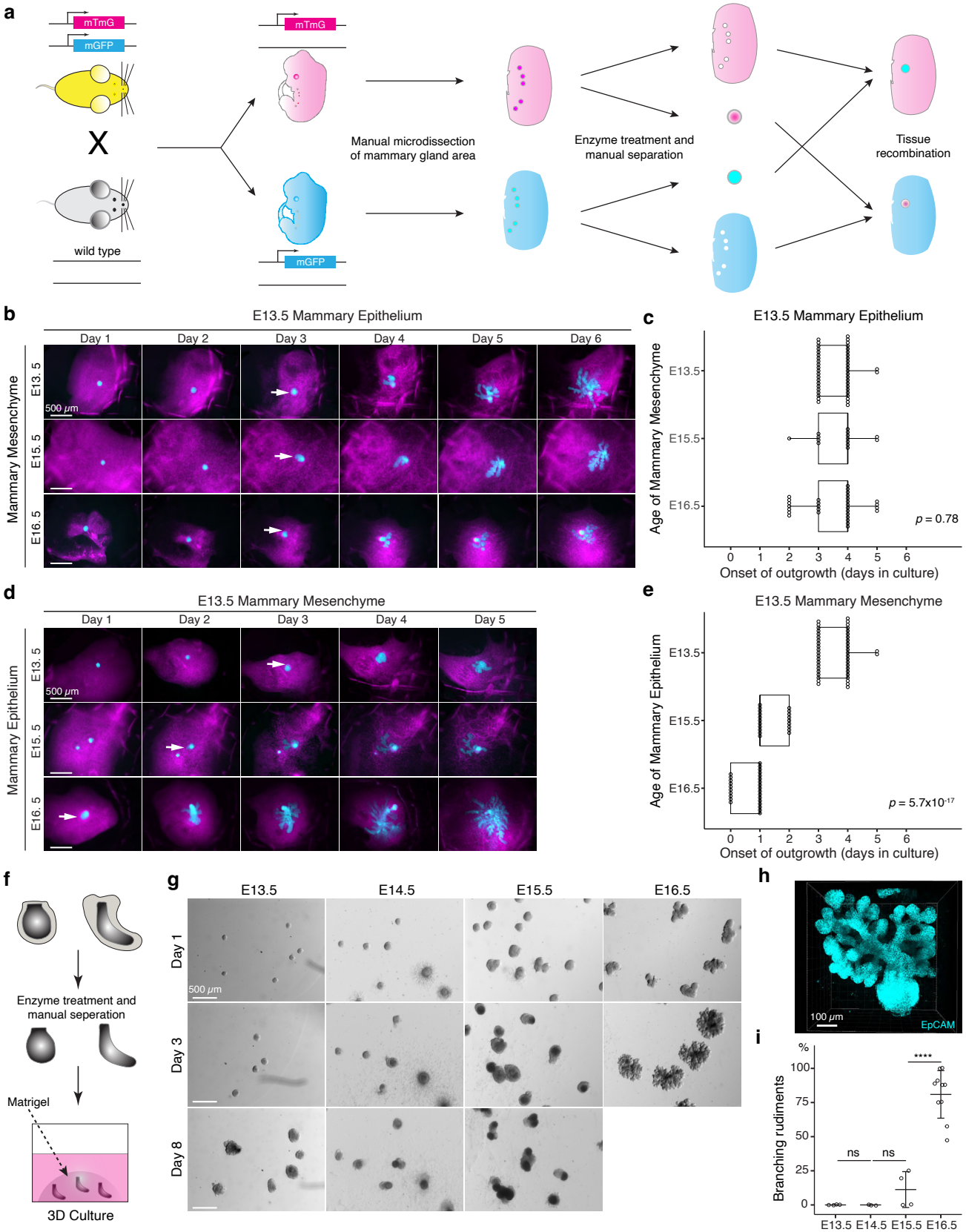
a
mTmG
mGFP
X
wild type
mTmG
mGFP
Manual microdissection of mammary gland area
Enzyme treatment and manual separation
Tissue recombination
b
E13.5 Mammary Epithelium
Day 1
Day 2
Day 3
Day 4
Day 5
Day 6
Mammary Mesenchyme
E13. 5
E15. 5
E16. 5
500 μm
c
E13.5 Mammary Epithelium
Age of Mammary Mesenchyme
E13.5
E15.5
E16.5
p = 0.78
0 1 2 3 4 5 6
Onset of outgrowth (days in culture)
d
E13.5 Mammary Mesenchyme
Day 1
Day 2
Day 3
Day 4
Day 5
Mammary Epithelium
E13. 5
E15. 5
E16. 5
500 μm
e
E13.5 Mammary Mesenchyme
Age of Mammary Epithelium
E13.5
E15.5
E16.5
p = 5.7x10-17
0 1 2 3 4 5 6
Onset of outgrowth (days in culture)
f
Enzyme treatment and manual seperation
Matrigel
3D Culture
g
E13.5
E14.5
E15.5
E16.5
Day 1
Day 3
Day 8
500 μm
h
100 μm
EpCAM
i
%
Branching rudiments
100
75
50
25
0
****
ns
ns
E13.5 E14.5 E15.5 E16.5

Fig. 1

Fig. 1 The timing of mammary gland outgrowth is an inherent property of the epithelium. a, A scheme illustrating the experimental procedure used in tissue recombination experiments. **b**, Representative images showing the onset of outgrowth of E13.5 mammary epithelia recombined with E13.5, E15.5, or E16.5 mammary mesenchymes, respectively. The appearance of the primary outgrowth is indicated with arrow. Scale bar, 500 μm. **c**, Quantification of the time (in days) required for onset of the branching. Data were pooled from 3-6 independent experiments of E13.5 mammary epithelia recombined with E13.5 (n=46 explants), E15.5 (n=14), and E16.5 (n=30) mammary mesenchymes. Statistical significance was assessed with the Kruskal–Wallis test. **d**, Representative images showing onset of outgrowth of E13.5, E15.5 and E16.5 mammary epithelia recombined with E13.5 mammary mesenchymes. The appearance of the primary outgrowth is indicated with arrow. Scale bar, 500 μm. **e**, Quantification of the time (in days) required for the onset of the primary outgrowth. Data were pooled from 3-6 independent experiments of E13.5 (n=46 explants), E15.5 (n=20) and E16.5 (n=27) mammary epithelia recombined with E13.5 mammary mesenchyme. Statistical significance was assessed with the Kruskal–Wallis test. **f**, A scheme illustrating the 3D culture of intact, mesenchyme-free epithelial mammary rudiments. **g**, Representative images showing the growth of E13.5, E14.5, E15.5 and E16.5 epithelial mammary rudiments in 3D culture; only E16.5 mammary rudiments were capable of branching (see also Supplementary Fig. 1). Scale bar, 500 μm. **h**, Representative 3D projection image of an EpCAM-stained E16.5 mammary rudiment after three days of 3D culture in Matrigel. Scale bar, 100 μm. **i**, Quantification of branching mammary rudiments in 3D culture. Data are presented as percentage of branching mammary rudiments (mean ± SD) from a total of 4 (E13.5), 3 (E14.5), 4 (E15.5), and 10 (E16.5) independent

experiments (each with minimum 6 rudiments in culture). The statistical significances were assessed using unpaired two-tailed Student's *t*-test with Bonferroni correction. ns, non-significant; ****, $p < 0.001$.

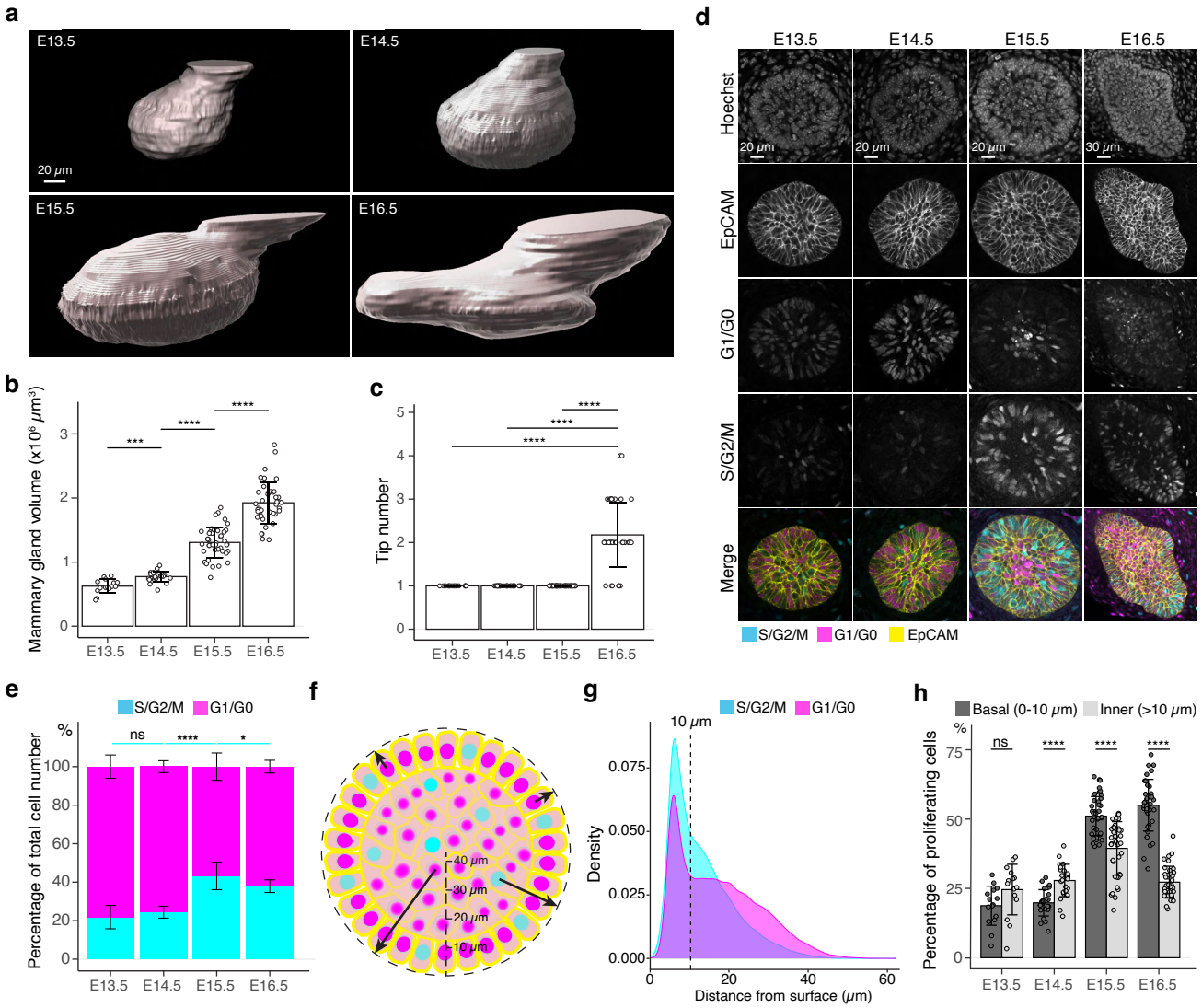
a
E13.5
E14.5
E15.5
E16.5
20 μm
b
Mammary gland volume (x10⁶ μm³)
c
Tip number
d
Hoechst
EpCAM
G1/G0
S/G2/M
Merge
20 μm
30 μm
S/G2/M
G1/G0
EpCAM
e
Percentage of total cell number
ns
f
40 μm
30 μm
20 μm
10 μm
g
10 μm
Density
Distance from surface (μm)
h
Basal (0-10 μm)
Inner (>10 μm)
Percentage of proliferating cells

Fig. 2

Fig.2 Cell cycle dynamics in embryonic mammary glands. a, Representative 3D surface rendering images of EpCAM-stained E13.5, E14.5, E15.5 and E16.5 epithelial mammary rudiments, based on 3D confocal imaging. Mammary gland 2 is shown. Scale bar, 20 μm. **b, c**, Quantification of epithelial mammary gland volume **(b)** and number of branching tips **(c)**, $n_{E13.5}$=15, $n_{E14.5}$=24, $n_{E15.5}$=41, $n_{E16.5}$=36. **d**, Confocal optical sections of whole mount-stained mammary glands from E13.5, E14.5, E15.5 and E16.5 Fucci2a embryos stained with EpCAM. Scale bars, 20 μm (E13.5-E15.5) and 30 μm (E16.5). **e**, Quantification of the proportions of all epithelial cells in S/G2/M and G1/G0 phases. Altogether, 15 glands (in total 9228 cells) from three E13.5 embryos, 24 glands (in total 17599 cells) from five E14.5 embryos, 41 glands (in total 40431 cells) from eight E15.5 embryos, and 36 glands (in total 50574 cells) from seven E16.5 embryos were analyzed. Data are presented as mean ± SD. **f**, A schematic image illustrating how the distance of cells (center of the nucleus) was quantified with respect to the surface of mammary rudiments. **g**, Density plot showing the distribution of the distance of nuclei in S/G2/M and G1/G0 phase to the surface of the mammary rudiment. Density plot revealed that a cluster of cells was localized within the distance of 10 μm (dashed line), which was set as the threshold to define “basal” and “inner” (luminal) cells. **h**, Quantification of the proportion of epithelial cells in S/G2/M phase in basal and inner compartments in E13.5-E16.5 epithelial mammary rudiments. Sample sizes are as in **e**. Data are presented as mean ± SD. The statistical significance was assessed using unpaired two-tailed Student’s *t*-test with Bonferroni correction. ns, non-significant; *, $p < 0.05$, ***, $p < 0.001$; ****, $p < 0.0001$.

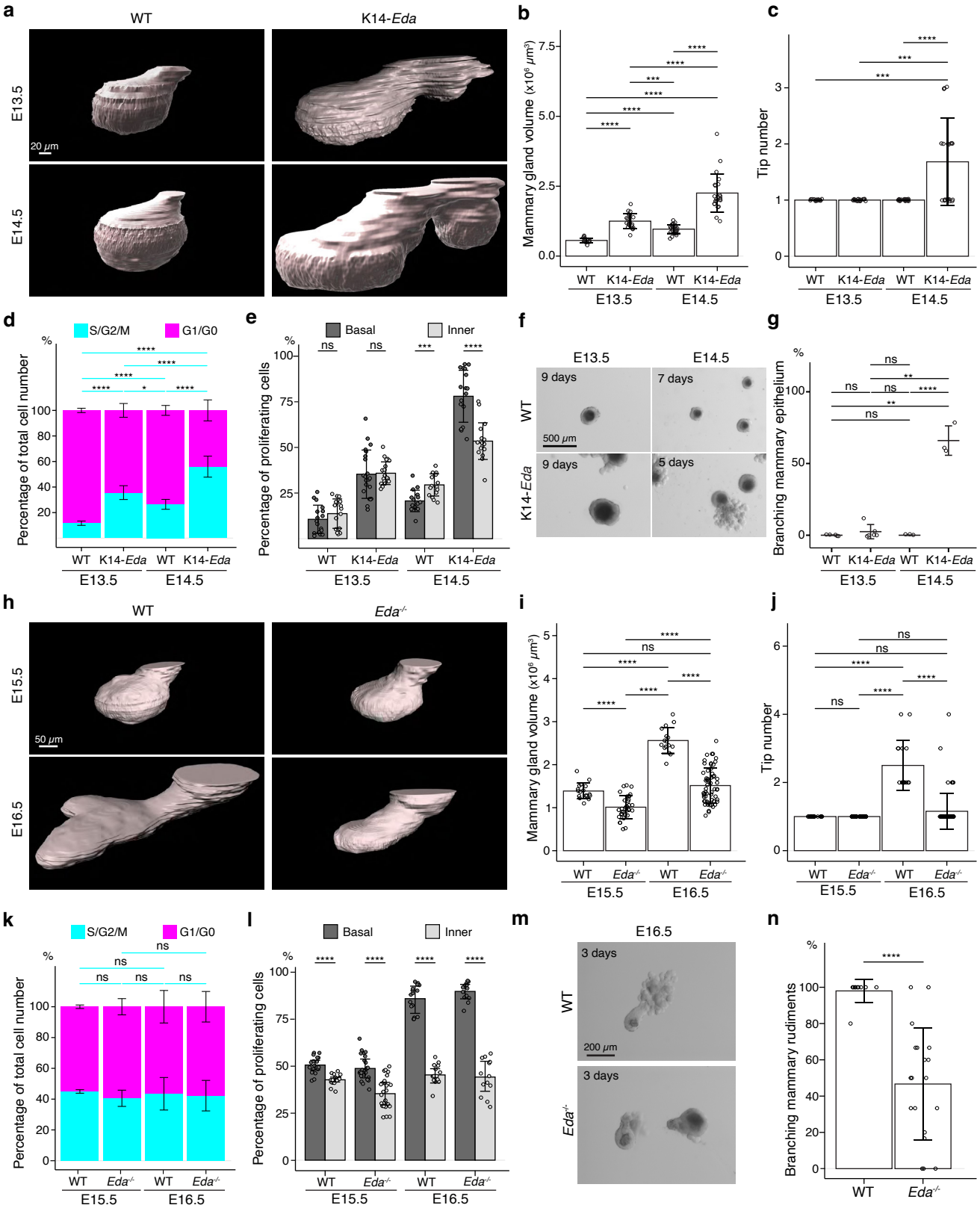
a
WT
K14-Eda
E13.5
E14.5
20 µm
b
Mammary gland volume (x10^6 µm^3)
WT K14-Eda WT K14-Eda
E13.5 E14.5
c
Tip number
WT K14-Eda WT K14-Eda
E13.5 E14.5
d
S/G2/M
G1/G0
Percentage of total cell number
WT K14-Eda WT K14-Eda
E13.5 E14.5
e
Basal
Inner
Percentage of proliferating cells
WT K14-Eda WT K14-Eda
E13.5 E14.5
f
E13.5
E14.5
9 days
7 days
9 days
5 days
500 µm
WT
K14-Eda
g
Branching mammary epithelium
WT K14-Eda WT K14-Eda
E13.5 E14.5
h
WT
Eda-/-
E15.5
E16.5
50 µm
i
Mammary gland volume (x10^6 µm^3)
WT Eda-/- WT Eda-/-
E15.5 E16.5
j
Tip number
WT Eda-/- WT Eda-/-
E15.5 E16.5
k
S/G2/M
G1/G0
Percentage of total cell number
WT Eda-/- WT Eda-/-
E15.5 E16.5
l
Basal
Inner
Percentage of proliferating cells
WT Eda-/- WT Eda-/-
E15.5 E16.5
m
E16.5
3 days
3 days
200 µm
WT
Eda-/-
n
Branching mammary rudiments
WT Eda-/-

Fig. 3

Fig.3 Basal-cell biased proliferation precedes, but is not sufficient to drive onset of branching. a, Representative 3D surface rendering images of EpCAM-stained mammary glands of K14-*Eda* embryos and their wild type (WT) littermates at E13.5 and E14.5. Mammary gland 2 is shown. Ectopic mammary rudiments (asterisk) common in K14-*Eda* embryos were excluded from the analysis. Scale bar, 20 μm. **b, c**, Quantification of mammary gland volume **(b)** and branching tip number **(c)** at E13.5 (n_{WT}= 17, $n_{K14\text{-}Eda}$= 21) and at E14.5 (n_{WT}= 16 and $n_{K14\text{-}Eda}$= 18). **d, e**, Quantification of the proportions of mammary epithelial cells in S/G2/M and G1/G0 phases in the entire epithelium (**d**) and the proportions of mammary epithelial cells in S/G2/M phase in basal and inner compartments (**e**) in WT or K14-*Eda* embryos at E13.5 (n_{WT}= 17 glands and in total 7714 cells from 3 embryos, $n_{K14\text{-}Eda}$= 21 glands and in total 15561 cells from 4 embryos) and E14.5 (n_{WT}= 16 glands and in total 10221 cells from 4 embryos, $n_{K14\text{-}Eda}$= 18 glands and in total 10520 cells from 5 embryos). **f**, Representative images showing the growth of E13.5 and E14.5 K14-*Eda* and wild type littermate epithelial mammary rudiments in 3D Matrigel culture. Note branching in E14.5 K14-*Eda* mammary rudiments. Scale bar, 500 μm. **g**, Quantification of branching mammary rudiments in 3D culture. Data are presented as percentage of branching mammary rudiments (mean ± SD) from a total of 4 (E13.5 WT), 6 (E13.5 K14-*Eda*), 3 (E14.5 WT) and 3 (E14.5 K14-*Eda*) independent experiments (each with minimum 5 rudiments in culture). **h**, Representative 3D surface rendering images of EpCAM-stained E15.5 and E16.5 epithelial mammary rudiments of *Eda*$^{-/-}$ and wild type embryos. Mammary gland 2 is shown. Scale bar, 50 μm. **i, j**, Quantification of epithelial mammary gland volume **(i)** and number of branching tips **(j),** at E15.5 (n_{WT} = 17 and $n_{Eda\text{-}/\text{-}}$ = 27) and at E16.5 (n_{WT} = 16 and $n_{Eda\text{-}/\text{-}}$ = 13). **k, l**, Quantification of the proportions of mammary epithelial cells in

S/G2/M or G1/G0 phases (**k**) and the proportions of mammary epithelial cells in S/G2/M phase in basal and inner compartments (**l**) in WT or *Eda*$^{-/-}$ embryos at E15.5 (n_{WT} = 17 glands and in total 14054 cells from 3 embryos, $n_{Eda-/-}$ = 27 glands and in total 21986 cells from 5 embryos) and E16.5 (n_{WT} = 16 glands and in total 40036 cells from 3 embryos, $n_{Eda-/-}$ = 13 glands and in total 22009 cells from 3 embryos). **m**, Representative images showing E15.5 and E16.5 *Eda*$^{-/-}$ and wild type epithelial mammary rudiments in 3D culture after 3 days. Scale bar, 200 μm. **n**, Quantification of branching mammary rudiments in 3D culture. Data are presented as percentage of branching mammary rudiments from a total of 6 WT and 18 *Eda*$^{-/-}$ E16.5 embryos (each with 3-6 rudiments in culture). Data are presented as mean ± SD. The statistical significance was assessed using unpaired two-tailed Student's *t*-test with Bonferroni correction. ns, non-significant; *, $p < 0.05$, **, $p < 0.01$, ***, $p < 0.001$; ****, $p < 0.0001$.

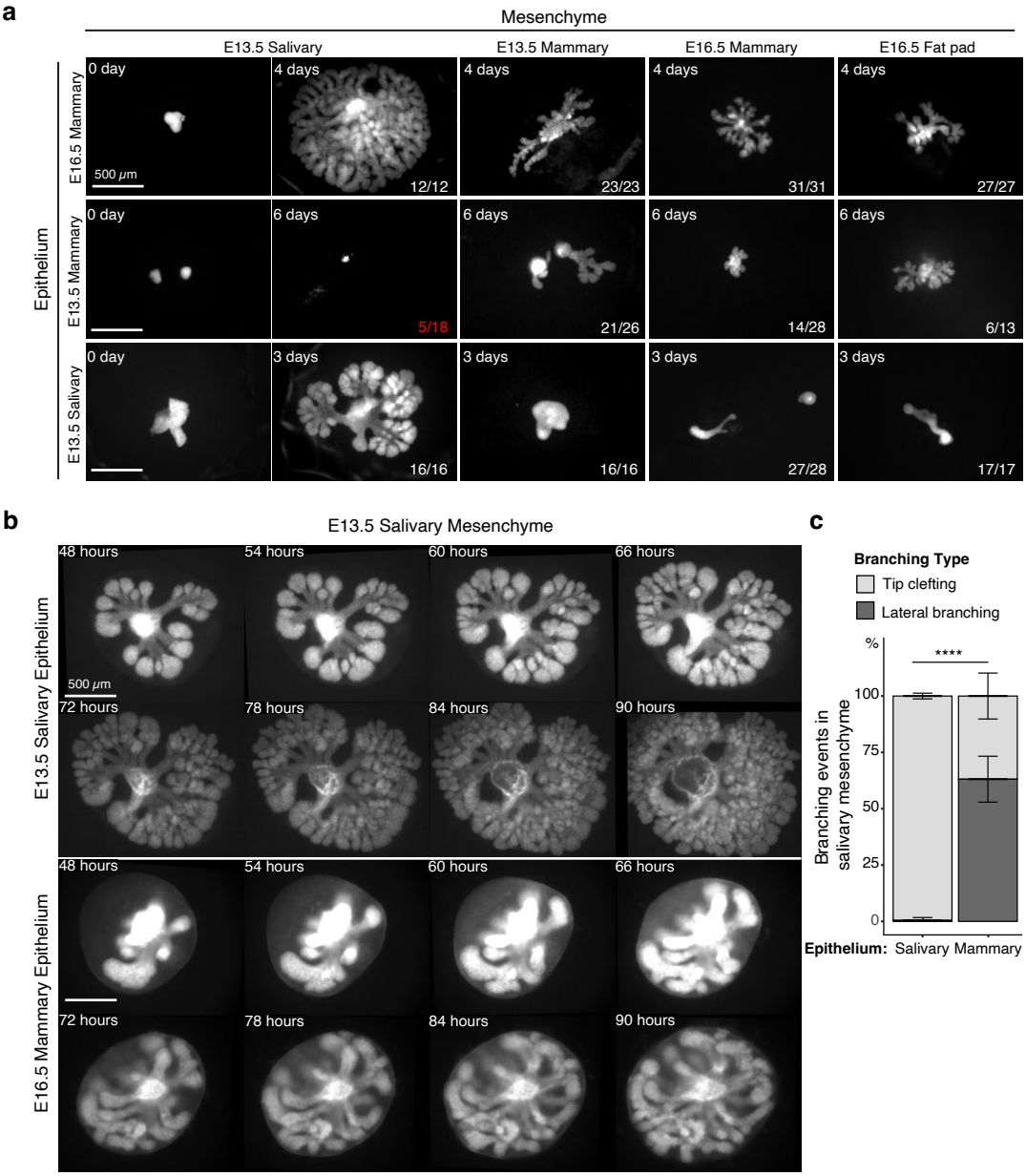
a
Mesenchyme
E13.5 Salivary
E13.5 Mammary
E16.5 Mammary
E16.5 Fat pad
Epithelium
E16.5 Mammary
E13.5 Mammary
E13.5 Salivary
0 day
4 days
500 μm
12/12
23/23
31/31
27/27
6 days
5/18
21/26
14/28
6/13
3 days
16/16
16/16
27/28
17/17
b
E13.5 Salivary Mesenchyme
E13.5 Salivary Epithelium
E16.5 Mammary Epithelium
48 hours
54 hours
60 hours
66 hours
72 hours
78 hours
84 hours
90 hours
c
Branching Type
Tip clefting
Lateral branching
%
****
Branching events in salivary mesenchyme
100
75
50
25
0
Epithelium: Salivary Mammary

Fig. 4

Fig. 4 Mammary mesenchyme is indispensable for the branching ability of the mammary gland. Recombination experiments between micro-dissected mammary and salivary gland tissues using fluorescently labeled epithelia (see also Fig.1). **a**, Representative images showing growth of the indicated epithelia recombined with distinct mesenchymes. Images were taken 0-6 days after culture as indicated in each figure. n in the lower right corner indicates growing recombinants out of those that survived, except for E13.5 mammary epithelium recombined with E13.5 salivary gland mesenchyme where it shows the number of survived recombinants/total recombinants (in red). In these recombinants, the epithelia never branched. Data were pooled from 3-4 independent experiments. Scale bars, 500 μm. **b**, Captions of time-lapse live imaging series of explants consisting of E13.5 salivary epithelium or E16.5 mammary epithelium recombined with E13.5 salivary mesenchyme. Images were captured every 2 hours starting 48h after recombination. The full video is provided as Supplementary Video 1. Scale bar, 500 μm. **c**, Quantification of the branching events (lateral branching and tip clefting) from time-lapse videos. A pooled data from three independent experiments: in total of 239 branching events from 9 control recombinants (salivary epithelium + salivary mesenchyme) and 159 branching events from 8 explants consisting of mammary epithelium and salivary gland mesenchyme were analyzed. Data are represented as mean ± SD and the statistical significance was assessed with unpaired two-tailed Student's *t*-test. *p* values: ****, $p < 0.0001$.

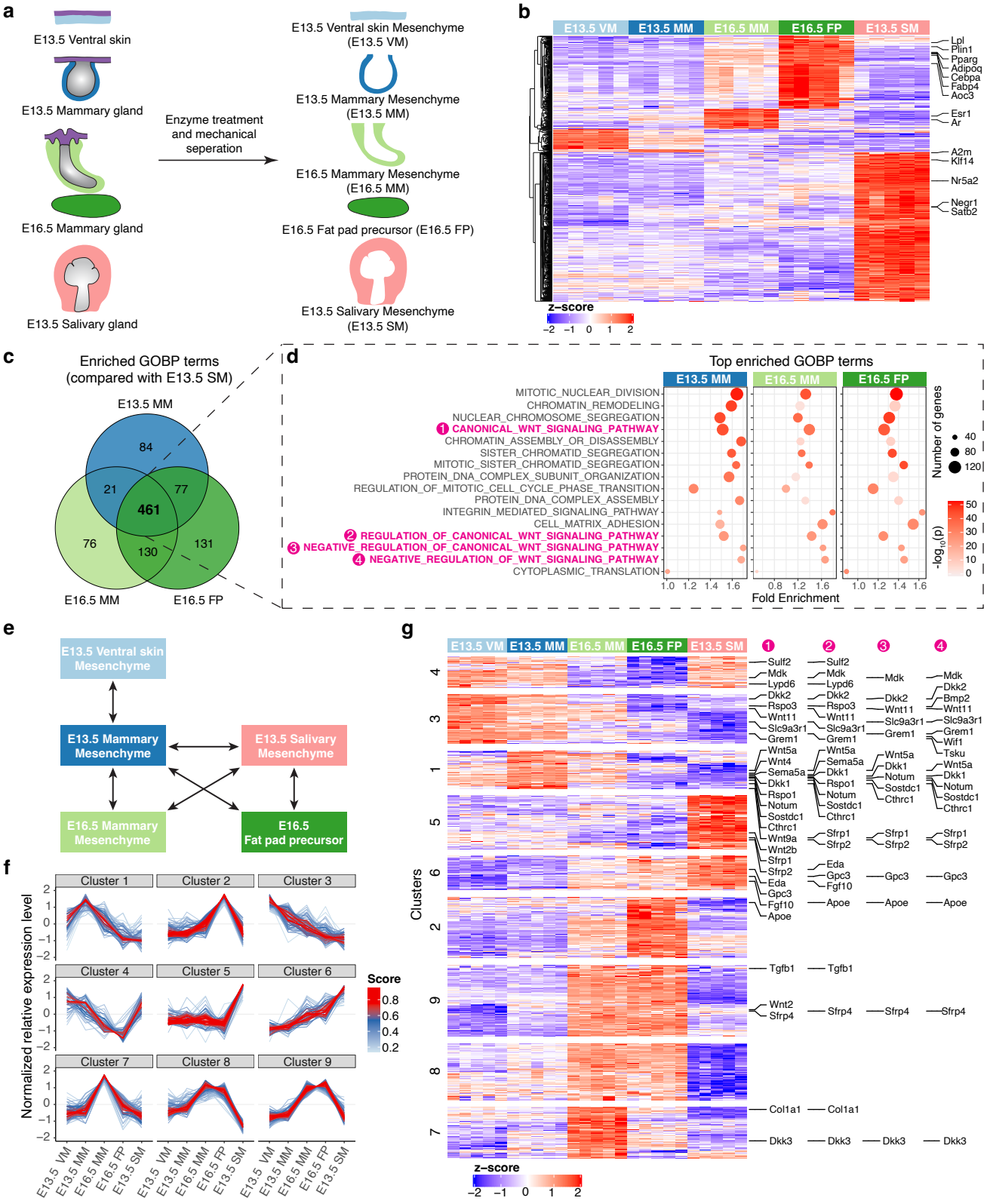
a
E13.5 Ventral skin
E13.5 Mammary gland
E16.5 Mammary gland
E13.5 Salivary gland
Enzyme treatment and mechanical seperation
E13.5 Ventral skin Mesenchyme (E13.5 VM)
E13.5 Mammary Mesenchyme (E13.5 MM)
E16.5 Mammary Mesenchyme (E16.5 MM)
E16.5 Fat pad precursor (E16.5 FP)
E13.5 Salivary Mesenchyme (E13.5 SM)
b
E13.5 VM
E13.5 MM
E16.5 MM
E16.5 FP
E13.5 SM
Lpl
Plin1
Pparg
Adipoq
Cebpa
Fabp4
Aoc3
Esr1
Ar
A2m
Klf14
Nr5a2
Negr1
Satb2
z-score
−2 −1 0 1 2
c
Enriched GOBP terms (compared with E13.5 SM)
E13.5 MM
84
21
77
461
76
130
131
E16.5 MM
E16.5 FP
d
Top enriched GOBP terms
E13.5 MM
E16.5 MM
E16.5 FP
MITOTIC_NUCLEAR_DIVISION
CHROMATIN_REMODELING
NUCLEAR_CHROMOSOME_SEGREGATION
1 CANONICAL_WNT_SIGNALING_PATHWAY
CHROMATIN_ASSEMBLY_OR_DISASSEMBLY
SISTER_CHROMATID_SEGREGATION
MITOTIC_SISTER_CHROMATID_SEGREGATION
PROTEIN_DNA_COMPLEX_SUBUNIT_ORGANIZATION
REGULATION_OF_MITOTIC_CELL_CYCLE_PHASE_TRANSITION
PROTEIN_DNA_COMPLEX_ASSEMBLY
INTEGRIN_MEDIATED_SIGNALING_PATHWAY
CELL_MATRIX_ADHESION
2 REGULATION_OF_CANONICAL_WNT_SIGNALING_PATHWAY
3 NEGATIVE_REGULATION_OF_CANONICAL_WNT_SIGNALING_PATHWAY
4 NEGATIVE_REGULATION_OF_WNT_SIGNALING_PATHWAY
CYTOPLASMIC_TRANSLATION
1.0 1.2 1.4 1.6
0.8 1.2 1.6
1.0 1.2 1.4 1.6
Fold Enrichment
Number of genes
40
80
120
-log10(p)
50
40
30
20
10
0
e
E13.5 Ventral skin Mesenchyme
E13.5 Mammary Mesenchyme
E13.5 Salivary Mesenchyme
E16.5 Mammary Mesenchyme
E16.5 Fat pad precursor
f
Normalized relative expression level
Cluster 1
Cluster 2
Cluster 3
Cluster 4
Cluster 5
Cluster 6
Cluster 7
Cluster 8
Cluster 9
Score
0.8
0.6
0.4
0.2
E13.5 VM
E13.5 MM
E16.5 MM
E16.5 FP
E13.5 SM
g
E13.5 VM
E13.5 MM
E16.5 MM
E16.5 FP
E13.5 SM
Clusters
4
3
1
5
6
2
9
8
7
Sulf2
Mdk
Lypd6
Dkk2
Rspo3
Wnt11
Slc9a3r1
Grem1
Wnt5a
Wnt4
Sema5a
Dkk1
Rspo1
Notum
Sostdc1
Cthrc1
Wnt9a
Wnt2b
Sfrp1
Sfrp2
Eda
Gpc3
Fgf10
Apoe
Tgfb1
Wnt2
Sfrp4
Col1a1
Dkk3
Bmp2
Wif1
Tsku
z-score
−2 −1 0 1 2

Fig. 5

Fig.5 Transcriptomic analysis identifying mesenchymal signals potentially regulating epithelial growth. a, A scheme illustrating the tissues isolated for RNAseq analysis. **b**, Heatmap showing the expression of the identified marker genes (with a threshold of average of normalized expression value in each group ≥ 100, fold change ≥ 2 and adjusted p-value < 0.05) in different mesenchymes using the z-score of log2-transformed normalized expression value (also see Supplementary Table 1). **c**, Venn diagram showing 461 enriched Gene Ontology Biological Process (GOBP) terms shared among E13.5 mammary mesenchyme (MM), E16.5 MM and E16.5 fat pad (FP) when compared to E13.5 salivary gland mesenchymes (SM) separately. **d**, Top 10 (among the 461 shared terms) of the most significantly enriched GOBP terms in each comparison resulted in 16 distinct terms in total. Four out of 16 terms were related to Wnt signaling pathway (in magenta). **e**, A scheme illustrating the pair-wise comparisons used to identify the genes with the potential to regulate epithelial growth. Altogether 644 genes encoding extracellular matrix proteins and ligands with average of normalized expression value in each group ≥ 200, fold change ≥ 1.5 and adjusted p-value < 0.05 were identified. **f**, mFuzzy cluster analysis of the genes identified in **e**. **g**, Heatmap showing the expression of genes identified in **e** using the z-score of log2-transformed normalized expression value. The clusters were defined by mFuzzy shown in **f**. The genes within the Wnt related GOBP terms identified in **d** are indicated accordingly in the right.

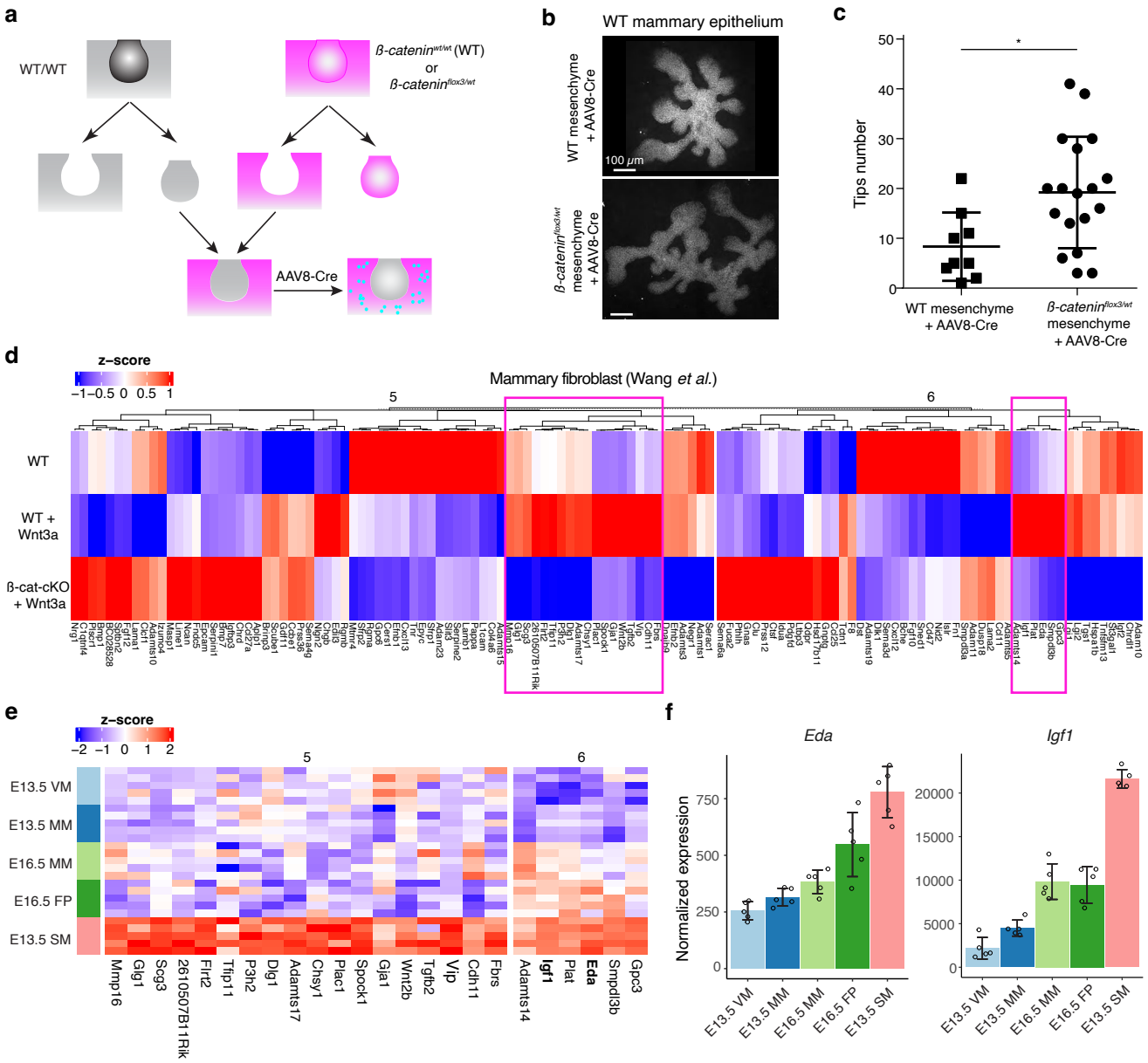
a
WT/WT
ß-catenin^wt/wt (WT)
or
ß-catenin^flox3/wt
AAV8-Cre
b
WT mammary epithelium
WT mesenchyme + AAV8-Cre
ß-catenin^flox3/wt mesenchyme + AAV8-Cre
100 μm
c
Tips number
WT mesenchyme + AAV8-Cre
ß-catenin^flox3/wt mesenchyme + AAV8-Cre
d
z-score
Mammary fibroblast (Wang et al.)
WT
WT + Wnt3a
ß-cat-cKO + Wnt3a
e
z-score
E13.5 VM
E13.5 MM
E16.5 MM
E16.5 FP
E13.5 SM
Mmp16
Glg1
Scg3
2610507B11Rik
Flrt2
Tfip11
P3h2
Dlg1
Adamts17
Chsy1
Plac1
Spock1
Gja1
Wnt2b
Tgfb2
Vip
Cdh11
Fbrs
Adamts14
Igf1
Plat
Eda
Smpdl3b
Gpc3
f
Eda
Igf1
Normalized expression
E13.5 VM
E13.5 MM
E16.5 MM
E16.5 FP
E13.5 SM

Fig. 6

Fig.6 Wnt-activated mesenchyme promotes growth of the mammary epithelium. a, A scheme illustrating the experimental design for mesenchymal activation of Wnt/ß-catenin signaling activity. **b**, Representative images showing EpCAM stained wild type mammary epithelia after 6 days culture in wild type or *ß-catenin*$^{flox3/wt}$ mesenchyme infected with AAV8-Cre virus during the first 48 hours. **c**, Quantification of the number of branching tips of wild type mammary epithelia recombined with wild type or *ß-catenin*$^{flox3/wt}$ mesenchyme after 6 days of culture. Data are presented as mean ± SD (n = 9 and 18 for WT and *ß-catenin*$^{flox3/wt}$ mesenchyme, respectively) and represented from three independent experiments. Statistical significance was assessed using unpaired two-tailed Student's *t*-test. *, $p < 0.05$. **d**, Unsupervised cluster of heatmap showing the expression of cluster 5 and 6 genes identified by mFuzzy analysis (see Fig. 5f) in a published dataset [42] that compared gene expression levels in wild type and *ß-catenin* deficient mammary fibroblasts cultured with or without Wnt3a protein. Data are shown as z-score of log2-transformed normalized expression values. Two subsets of potential mesenchymal Wnt target genes identified are marked (box in magenta). **e**, Heatmap showing the expression of the candidate genes from **d** in different mesenchymes of the RNAseq data. Data are shown as z-score of log2-transformed normalized expression values. **f**, Graphs representing mRNA expression of *Eda* and *Igf1* as measured by RNAseq. Data are presented as normalized expression values (mean ± SD). Each dot represents one biological replicate.

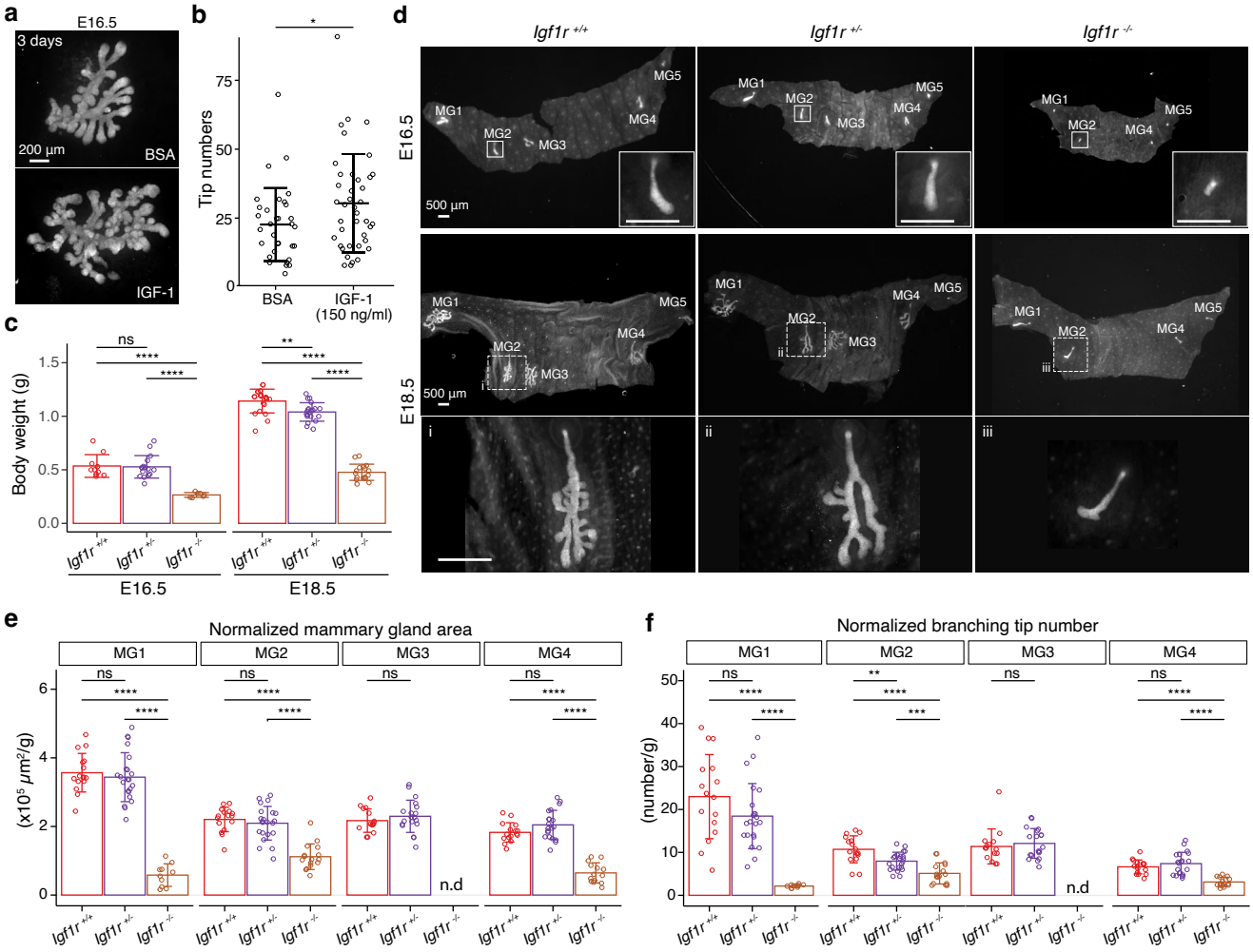
a
E16.5
3 days
200 µm
BSA
IGF-1
b
Tip numbers
BSA
IGF-1
(150 ng/ml)
c
Body weight (g)
E16.5
E18.5
d
Igf1r +/+
Igf1r +/-
Igf1r -/-
E16.5
E18.5
MG1
MG2
MG3
MG4
MG5
500 µm
e
Normalized mammary gland area
(x10^5 µm^2/g)
n.d
f
Normalized branching tip number
(number/g)
n.d

Fig. 7

Fig. 7 IGF-1R is required for embryonic mammary gland development and branching morphogenesis. a, Representative images of E16.5 K14-Cre::mTmG mammary glands cultured *ex vivo* for three days in the presence of 150 ng/ml recombinant IGF-1 or vehicle (BSA). Scale bar, 200 µm. **b**, Quantification of the number of branching tips in vehicle (n=33) and IGF-1 treated (n=40) mammary gland explants. Data are pooled from 5 independent experiments and presented as mean ± SD. Statistical significance was assessed using unpaired two-tailed Student's *t*-test. *, $p < 0.05$. **c**, Body weight of *Igf1r*$^{+/+}$, *Igf1r*$^{+/-}$ and *Igf1r*$^{-/-}$ embryos at E16.5 ($n_{Igf1r+/+}$=10, $n_{Igf1r+/-}$=16; $n_{Igf1r-/-}$=7), and E18.5 ($n_{Igf1r+/+}$=20, $n_{Igf1r+/-}$=20; $n_{Igf1r-/-}$=17). Data are presented as mean ± SD. Statistical significances were calculated with unpaired two-tailed Student's *t*-test with Bonferroni correction. ns, non-significant; **, $p < 0.01$; ****, $p < 0.0001$. **d**, Representative images of EpCAM-stained ventral skin including mammary glands (MG) 1-5 from *Igf1r*$^{+/+}$, *Igf1r*$^{+/-}$ and *Igf1r*$^{-/-}$ female embryos at E16.5, and E18.5. Note absence of MG3 in *Igf1r*$^{-/-}$ embryos. Magnifications show mammary gland 2. Scale bars, 500 µm. **e, f**, Quantification of mammary gland area **(e)** and number of branch tips **(f)** normalized to body weight in *Igf1r*$^{+/+}$, *Igf1r*$^{+/-}$ and *Igf1r*$^{-/-}$ embryos at E18.5. MG5 was often lost during dissection and therefore was not included in the analysis. n.d, not detected. Data are presented as mean ± SD and the statistical significances were assessed using unpaired two-tailed Student's *t*-test with Bonferroni correction. ns, non-significant; *, $p < 0.05$, **, $p < 0.01$, ***, $p < 0.001$; ****, $p < 0.0001$.

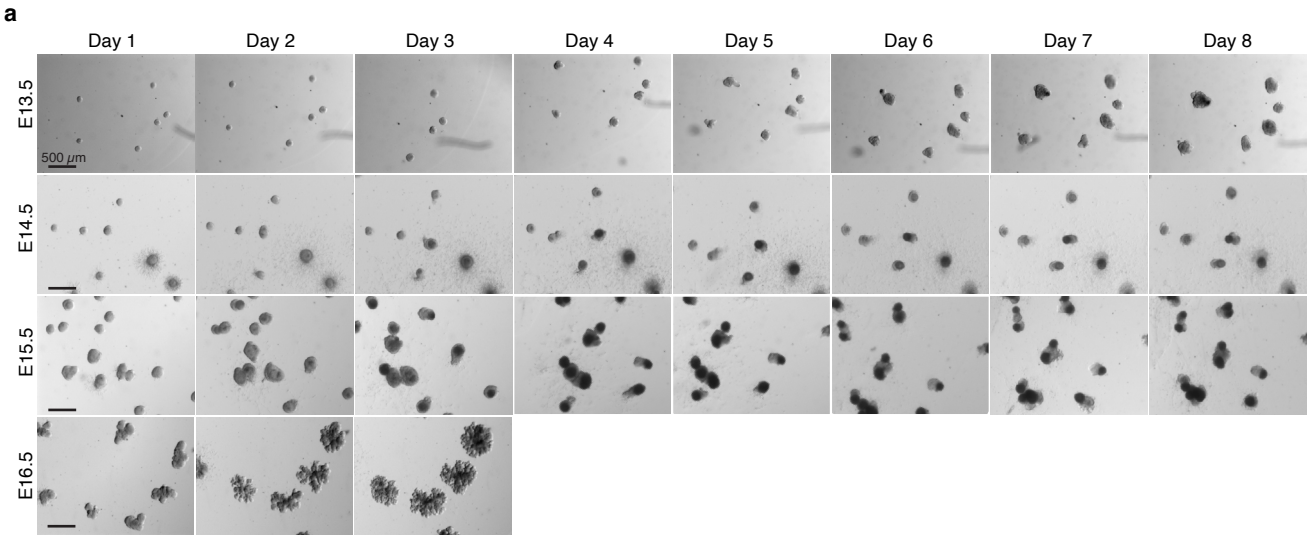

Supplementary Fig. 1

Supplementary Fig.1 Epithelial mammary rudiments isolated from stages earlier than E16.5 are not able to branch in 3D culture. Representative images showing the growth of E13.5, E14.5, E15.5 and E16.5 epithelial mammary rudiments 1 in 3D Matrigel culture. Images were acquired once per day. Scale bar, 500 μm.

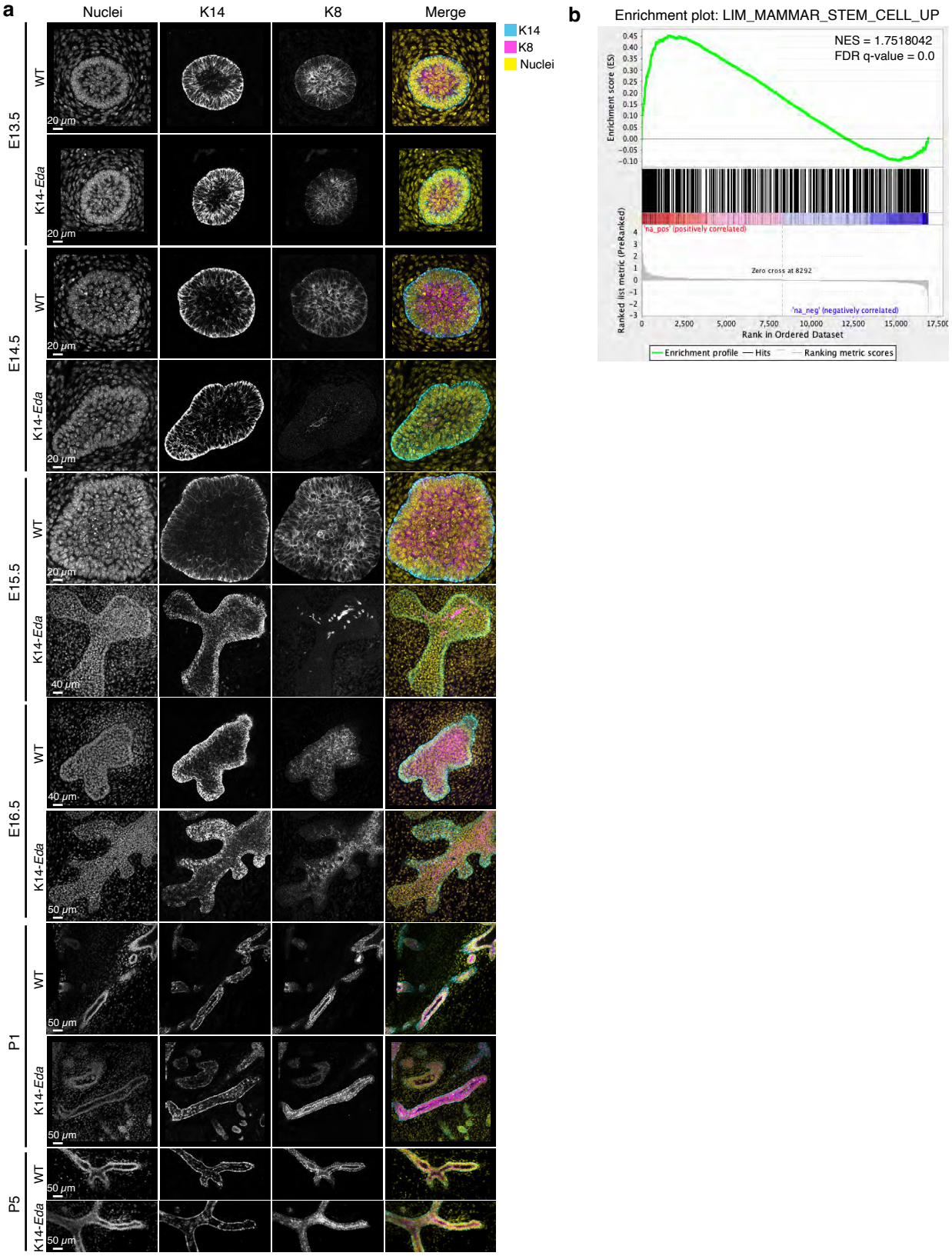

Supplementary Fig. 2

Supplementary Fig. 2 Overexpression of Eda transiently suppresses the luminal cell fate. a, Confocal optical sections of whole mount imaged E13.5, E14.5, E15.5, E16.5, postnatal day 1 (P1), and P5 wild type and K14-*Eda* mammary glands stained with the basal marker K14 (Cyan in merged images) and luminal marker K8 (Magenta in merged images). Nuclei were visualized with Hoechst. Mammary glands from at least 3 embryos from 2-3 litters were examined in each condition. Scale bars, 20-50 μm as indicated in the figures. **b**, Gene set enrichment analysis of Voutilainen data [29] of E13.5 *Eda*$^{-/-}$ mammary buds treated with recombinant Eda protein for 4 hours revealed a positive enrichment of 'LIM_Mammary_Stem_Cell_Up' gene signature [30].

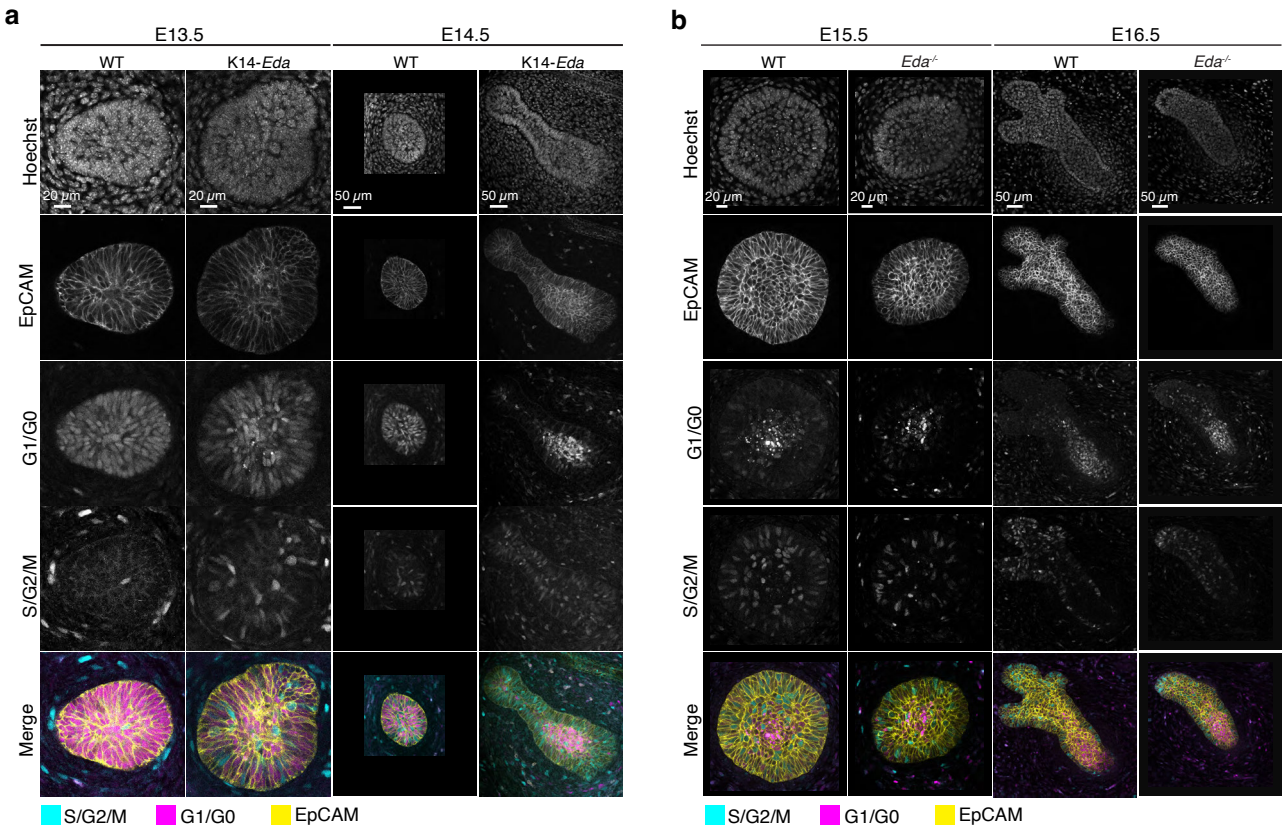

Supplementary Fig. 3

Supplementary Fig. 3 The proliferation dynamics of mammary epithelium in *Eda* gain-of-function and loss-of-function mouse models. a, Confocal optical sections of whole-mount mammary glands from E13.5 and E14.5 K14-*Eda* or WT littermate embryos expressing Fucci2a reporter stained with EpCAM. Scale bars, 20 μm (E13.5) and 50 μm (E14.5). **b**, Confocal optical sections of whole-mount mammary glands from E15.5 and E16.5 WT or *Eda*$^{-/-}$ Fucci2a embryos stained with EpCAM. Scale bars, 20 μm (E15.5) or 50 μm (E16.5).

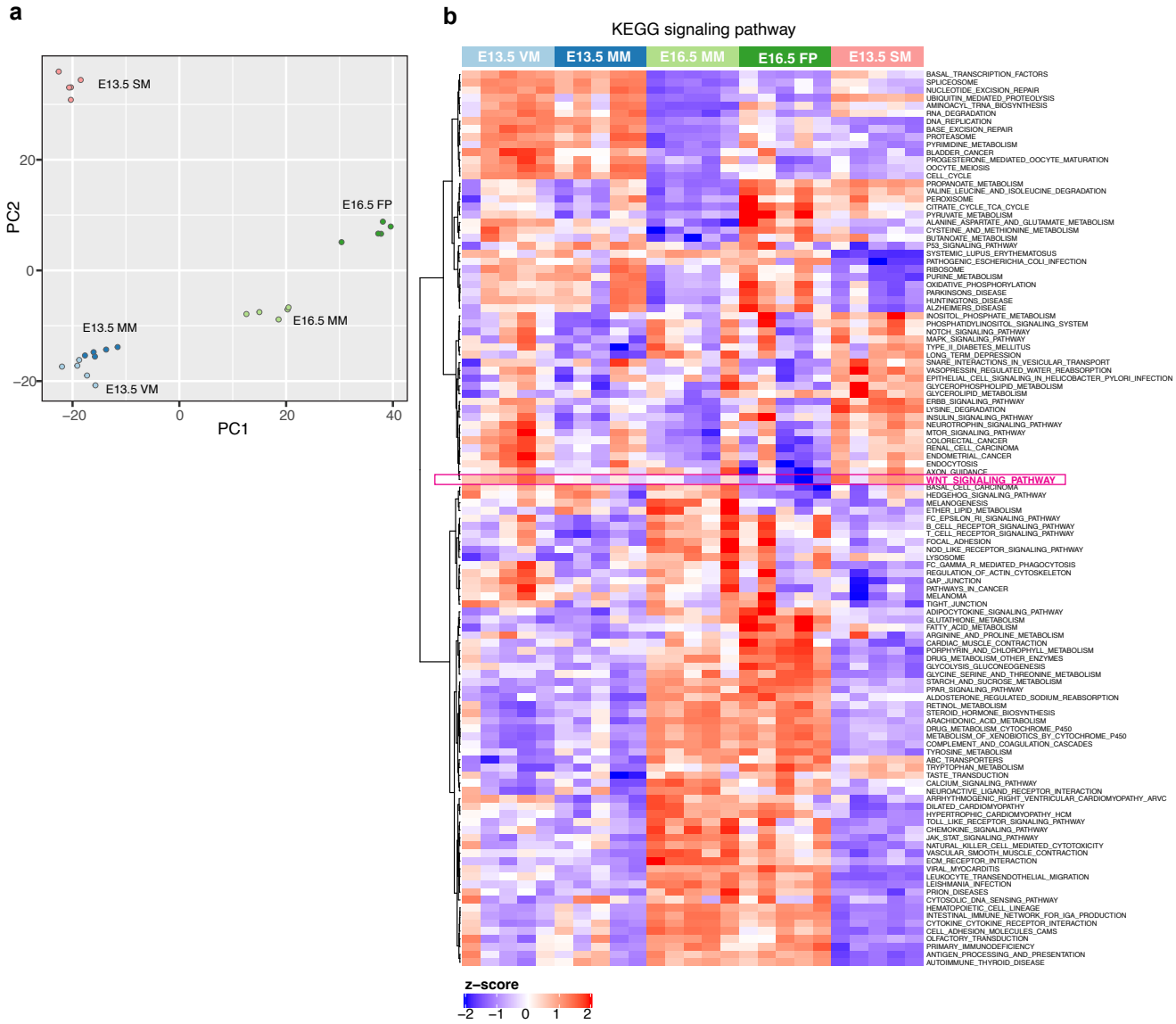

Supplementary Fig.4

Supplementary Fig 4. Transcriptomic profiling of different mesenchymes. a, Scatter plot shows the principal component analysis of E13.5 ventral skin mesenchyme (VM), E13.5 mammary mesenchyme (MM), E16.5 MM, E16.5 fat pad (FP), and E13.5 salivary gland mesenchyme (SM). **b**, Heatmap shows the significantly altered KEGG signaling pathways comparing E13.5 MM, E16.5 MM or E16.5 FP with E13.5 SM separately. WNT_SIGNALING_PATHWAY (marked with Magenta) is low in E16.5 MM and E16.5 FP compared to other tissues.

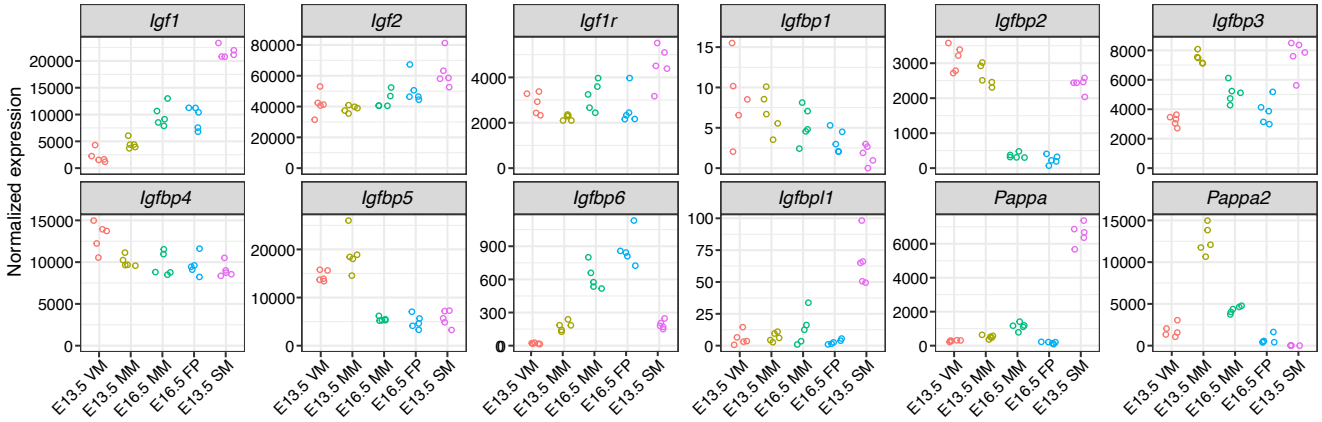

Supplementary Fig. 5

Supplementary Fig. 5. Expression of IGF pathway genes in the mesenchymal tissues.

Graphs show mRNA expression of the indicated genes by RNAseq in E13.5 ventral, non-mammary skin mesenchyme (VM), E13.5 mammary mesenchyme (MM), E16.5 MM, E16.5 fat pad precursor (FP), and E13.5 salivary gland mesenchyme (SM). Each dot represents one biological replicate.

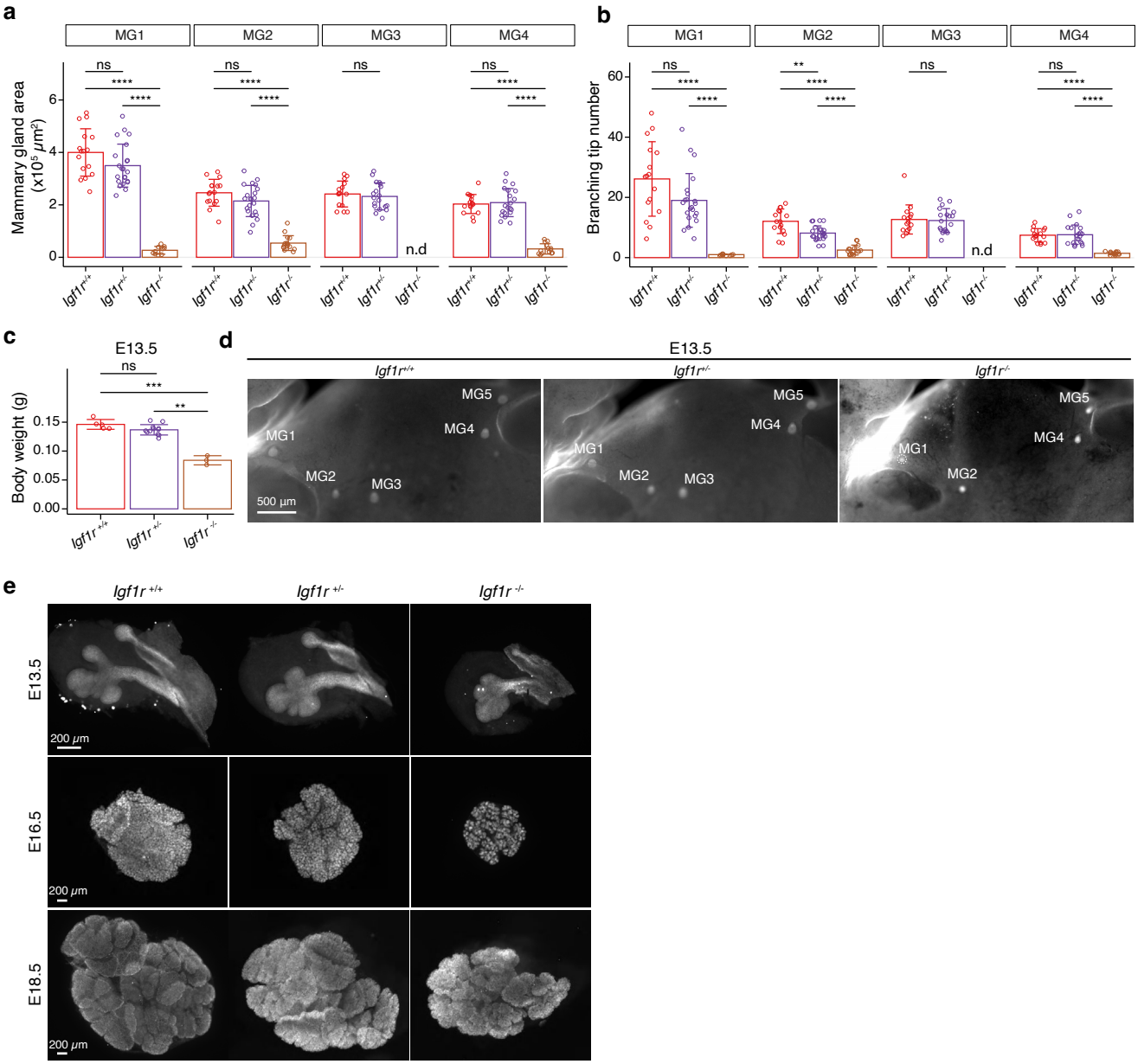

Supplementary Fig. 6

Supplementary Fig. 6. Impact of *Igf1r* deficiency on mammary gland and salivary gland growth and branching. **a, b,** Quantification of mammary gland area **(a)** and tip number **(b)** of E18.5 *Igf1r*$^{+/+}$, *Igf1r*$^{+/-}$ and *Igf1r*$^{-/-}$ female embryos. Samples are the same as in Fig. 7e,f. Data are presented as mean ± SD. **c**, Body weight of *Igf1r*$^{+/+}$, *Igf1r*$^{+/-}$, and *Igf1r*$^{-/-}$ embryos at E13.5 ($n_{Igf1r+/+}$=5, $n_{Igf1r+/-}$=13; $n_{Igf1r-/-}$=3). Data are presented as mean ± SD. **d**, Representative images of EpCAM-stained E13.5 embryos showing mammary glands (MG) 1-5 from *Igf1r*$^{+/+}$, *Igf1r*$^{+/-}$ and *Igf1r*$^{-/-}$ embryos. Scale bar, 500 μm. **e,** Representative images of EpCAM-stained *Igf1r*$^{+/+}$, *Igf1r*$^{+/-}$, and *Igf1r*$^{-/-}$ salivary glands at E13.5 ($n_{Igf1r+/+}$=6, $n_{Igf1r+/-}$=8; $n_{Igf1r-/-}$=20), E16.5 ($n_{Igf1r+/+}$=15, $n_{Igf1r+/-}$=29; $n_{Igf1r-/-}$=5), and E18.5 ($n_{Igf1r+/+}$=6, $n_{Igf1r+/-}$=13; $n_{Igf1r-/-}$=6). Scale bars, 200 μm. Statistical significances were assessed using unpaired two-tailed Student's *t*-test with Bonferroni correction. ns, non-significant; *, $p < 0.05$, **, $p < 0.01$, ***, $p < 0.001$; ****, $p < 0.0001$.

Supplementary Table 1. The list of identified marker genes for each mesenchyme and their normalized expression value in each sample.

Supplementary Table 2. The results of mFuzzy analysis shown in Fig. 5f and the normalized expression value of each gene in each sample.

Supplementary Video 1. Time-lapse live imaging showing the growth of E13.5 salivary epithelium (left) and E16.5 mammary epithelium (right) in E13.5 salivary mesenchyme. Images were captured every 2 hours starting 48h after recombination. Scale bar, 500 μm.